Paleomagnetism of the lower two unconformity-bounded sequences of the Waterberg Group, South Africa: Towards a better-defined apparent polar wander path for the Paleoproterozoic Kaapvaal Craton.

M.O. de Kock
Paleoproterozoic Mineralization Research Group, University of Johannesburg,
P.O. Box 524, Auckland Park, 2006, South Africa
e-mail: glgy5@na.rau.ac.za

D.A.D. Evans
Department of Geology and Geophysics, Yale University, P.O. Box 208109, New Haven,
CT 065208109, United States of America
e-mail: dai.evans@yale.edu

H.C. Dorland, N.J. Beukes and J. Gutzmer
Paleoproterozoic Mineralization Research Group, University of Johannesburg,
PO Box 524, Auckland Park, 2006, South Africa
e-mail: HCDorland@yahoo.com, njb@rau.ac.za, jg@rau.ac.za

ABSTRACT

Paleomagnetic data from more than 250 samples of the lower part of the Waterberg Group (Nylstroom Subgroup) are reported in order to reevaluate the apparent polar wander path (APWP) of the Kaapvaal craton during the Paleoproterozoic Era. Our study broadly confirms the established APWP, but reveals some previously unidentified complexities in the time interval ~2.05 Ga to ~1.87 Ga. A primary remanence direction from the lower part of the Swaershoek Formation provides a paleomagnetic pole of (36.5° north, 051.3° east, K = 23.4, A_{95} = 10.9) for the Waterberg unconformity-bounded sequence I (WUBS-I) at ~2.05 Ga. A large shift in pole position takes place from the lower Swaershoek into the upper Swaershoek Formation and overlying Alma Formation of Waterberg unconformity-bounded sequence II (WUBS-II; pole at -10.5° north, 330.4° east, K = 25.0, A_{95} = 9.8), confirming the existence of a major unconformity and/or rapid continental motion within the span of Swaershoek deposition.

Introduction

The Waterberg Group of South Africa, together with the Soutpansberg Group, Palapye Group, Olifantshoek Supergroup, and Blouberg succession, and a number of small outliers, are erosional remnants of extensive redbed successions that developed on the Kaapvaal craton and its margins during the Paleoproterozoic. Although outlines of the apparent polar wander path (APWP) for the Paleoproterozoic Kaapvaal craton have been proposed for decades (*e.g.*, Morgan and Briden, 1981), some poles are debated (see for example the discussion on the Bushveld Complex paleopoles in Evans *et al.*, 2002, and Hanson *et al.*, 2004a). Paleomagnetic sampling of the Waterberg Group has been undertaken in the past (see discussion below), but the use of now-outdated demagnetization techniques, particularly the lack of statistically robust field tests, and absence of reliable numerical age data have rendered much of the previous work questionable. This study seeks to refine the APWP for Paleoproterozoic Kaapvaal craton with high-reliability paleomagnetic poles from the lower Waterberg succession.

Regional Geology

The predominantly clastic Waterberg Group is part of a Paleoproterozoic redbed succession that is widespread across southern Africa. The major Waterberg outcrop area (Figure 1a) is mostly confined to the Limpopo Province but also exists partly in the Northwest Province with some extension into the eastern part of Botswana. Another outcrop area, the so-called Middelburg "basin", is situated mostly in Mpumalanga and Gauteng Provinces around the cities of Middelburg and Cullinan. Located between the northern area and the Middelburg area is the small erosional outlier of Rust de Winter that correlates with the lower Waterberg Group (Dorland *et al.*, 2006). The Waterberg Group rests in all three areas unconformably on the Rooiberg Group, which has a U-Pb zircon age of 2061 ± 2 Ma (Walraven, 1997).

The Waterberg Group is divided into the Nylstroom, Matlabas, and Kranskop Subgroups (SACS: South African Committee for Stratigraphy, 1980) and informally into the "Lower" and "Upper" Waterberg Group based upon outcrop distribution (Jansen, 1982). The Matlabas and Kranskop Subgroups comprise the "Upper" Waterberg succession. In contrast to this subdivision, Cheney and Twist (1986) divided the Waterberg Group into five unconformity-bounded sequences (Figure 1b).

Jansen (1982) divided the large northern outcrop area into the Nylstroom "basin" and the Main "basin"

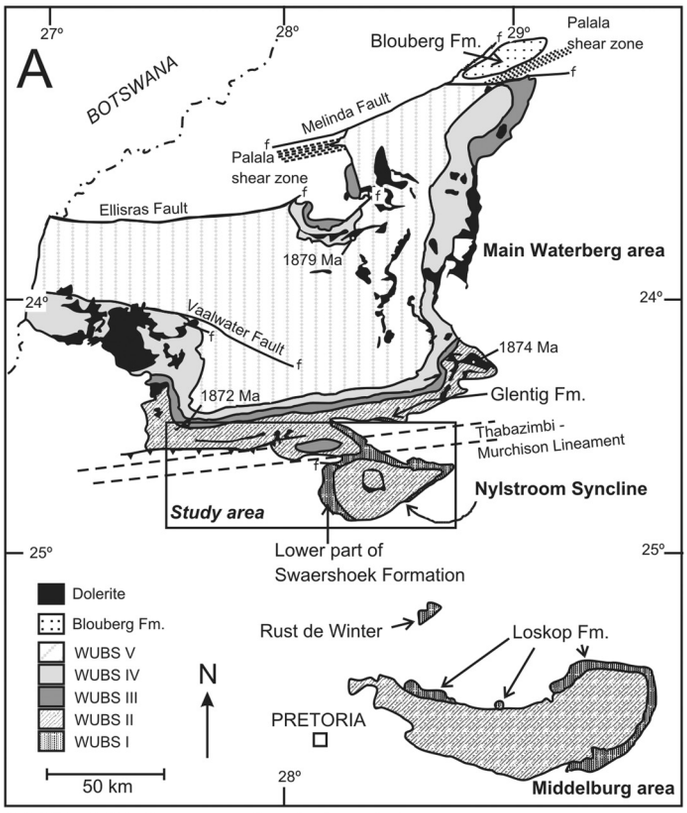

WUBS = Waterberg unconformity-bounded sequence

B

Kanye (Botswana)	Middelburg	Rust de Winter	Nylstroom	Waterberg SSW	Waterberg SE & Central	Waterberg NNE	Blouberg	WUBS
				Vaalwater Formation				
				Cleremont Formation				V
				Sandriviersberg Formation		Mogalakwena Formation		
				Aasvoëlkop Formation		Makgabeng Formation		IV
Mannyelanong Hill Fm.	Skilpadkop Fm. erosional remnant			Skilpadkop Formation		Setlaole Formation	Blouberg Formation	III
Otse Group	Wilgerivier Formation		Alma Formation	"Upper" Swaershoek Formation	Sterk-rivier Formation			II
	Loskop Formation	Rust de Winter Formation	"Lower" Swaershoek Formation		Glentig Formation			I
Moshaneng Complex	Rooiberg Group						Palala shear zone	

WUBS = Waterberg unconformity-bounded sequence

Nylstroom Subgroup Matlabas Subgroup Kranskop Subgroup

Figure 1 (**a**) Simplified geological map showing the distribution of the five unconformity-bounded sequences of the Waterberg Group (modified after Cheney and Twist 1986). The distribution of ~1.88 Ga dolerite sills is also shown. Age dates are U-Pb baddelyite ages from Hanson *et al*. (2004) (**b**) Stratigraphic subdivision and correlation of the Waterberg Group, compiled from Hanson *et al*. (2004a) and Cheney and Twist (1986).

(Figure 1a). Callaghan *et al.* (1991) provided an overview of the Main "basin" area. The Nylstroom Subgroup mostly crops out in the so-called Nylstroom "basin" (Figure 2) as a distinctive pear-shaped attachment to the Main Waterberg "basin". This structure is known as the Nylstroom Syncline and was thought to have initially formed during a proto-basinal phase in the development of the Waterberg basin (Jansen, 1982), but use of the term proto-basin was argued against by Cheney and Twist (1986), who stated that the observed outcrop distribution is the result of favored preservation of the sequence in structural lows such as the Nylstroom Syncline. Du Plessis (1987) also disagreed with the idea of a proto-basin and instead argued that the Nylstroom area represents an early phase of the developing Waterberg pull-apart basin. The lower part of the Swaershoek Formation is equated by Cheney and Twist (1986) to the Loskop and Glentig Formations of the Middelburg area and southeastern part of the Main Waterberg "basin" respectively and represents the oldest of their five proposed unconformity-bounded sequences (Figure 1b). However, they did not regard this sequence as forming part of the Waterberg succession.

In the Nylstroom area and the south-southwestern parts of the Main "basin" the Nylstroom Subgroup is divided into the Swaershoek and Alma Formations (SACS: South African Committee for Stratigraphy, 1980). Jansen (1982) described the oldest Swaershoek beds as being developed in the northwestern portion of the Nylstroom Syncline, where they comprise dominantly red clastic sediments and some quartz porphyry flows (including the unit dated by Dorland *et al.*, 2006). This is followed by sandstone and conglomerate, including the spectacular boulder conglomerate interpreted to represent the boundary between Waterberg unconformity-bounded sequences (WUBS) I and II. The upper part of the Swaershoek Formation consists of sandstone, with subordinate trachytic lava and shale. Resting conformably on the Swaershoek, the Alma Formation is generally composed of arenaceous and feldspathic fine wackestones.

The age of the Waterberg Group is reviewed by Dorland, *et al.* (2006) and can be constrained between 2054 ± 4Ma, the age of a quartz porphyry lava near the base of the Swaershoek Formation (Dorland *et al.*, 2006), and ~1.88 to ~1.87 Ga, the oldest precise ages from dolerite sills intruding the Waterberg Group (Hanson *et al.*, 2004a).

Previous paleomagnetic work

Purple and red strata of the Waterberg Group (from localities in the Nylstroom area and Middelburg area) and Soutpansberg Group, in an early paleomagnetic study by Jones and McElhinny (1967), yielded a range of site directions that generally fell into distinct groups. The observed groupings were stratigraphically coherent, with sites from similar stratigraphic levels tending to group together. McElhinny (1968) arranged the site means into five groups. The older three of these groups were abbreviated by Morgan and Briden (1981) as W1 to W3, a usage that was employed by many subsequent workers. The W1 and W3 poles include sites from the Middelburg area and the Nylstroom area, while the W2 pole is based on a sampling site from the Soutpansberg area and is denoted by Jones and McElhinny (1967) as originating from the so-called "Loskop System". The rocks at the sampling site are currently mapped as belonging to the Nzhelele Formation (Council for Geoscience, 1997). The Nzhelele Formation supersedes lavas of the Sibasa Formation that are tentatively correlated with post-Waterberg dolerite at ~1.88 Ga Ma (Hanson *et al.*, 2004a); thus W2 should in fact post-date both W1 and W3. Morgan and Briden (1981) also sampled red beds and acid volcanics in the Rust de Winter outlier. Whereas the acid volcanics yielded no significant mean directions, the red beds did yield a characteristic component with intermediate-level demagnetization spectra, directed between W1 and W2. A recent study (Maré *et al.*, 2006) investigated the paleomagnetism of the Swaershoek (Nylstroom region) and Wilgeriver (Middelburg area) Formations, and also of post-Waterberg dolerite intrusions. This study found the poles of the Waterberg red beds significantly displaced from that of the dolerites to rule out pervasive overprinting by the intrusions. Maré *et al.* (2006) could not, however, rule out overprinting at another stage. Unfortunately, none of the paleomagnetic directions obtained from the Waterberg red beds thus far are constrained by field tests, and as is typical of older studies, adequate demagnetization techniques such as vector subtraction or principal component analysis are commonly lacking.

Sampling and analytical techniques

We sampled the Nylstroom Subgroup in the Nylstroom "basin" for paleomagnetic study (see Figure 2 for localities). The Swaershoek Formation was sampled at five localities, with in some cases up to seven sampling sites per locality. Most localities provided one or more possible field tests for paleomagnetic stability. Stratigraphically (Figure 3), the sampling sites are representative of the lower (SWC, SWE and SWF) and upper (SWB, SWD) parts of the Swaershoek Formation, which is informally divided by the sporadic appearance of trachytic lava in the upper unit (Jansen, 1982). The Alma Formation was sampled along a profile at Bakker's Pass; this profile (ABP 1-70) traversed a post-Waterberg sill, which was sampled for a baked contact test. Another post-Waterberg sill, the Nylstroom sill, was sampled at two sites (NYLA and B). East of Bakker's Pass, a few samples were collected from the overlying Aasvoëlkop Formation (ABP 71-78). Pebble- to cobble-sized clasts of fine-grained sediments likely sourced from the Alma Formation were sampled from the Skilpadkop Formation for a conglomerate test (SKIL).

Oriented samples were collected in the field with a portable, hand-held petrol drill. Orientation was achieved by magnetic compass, and for most samples, a

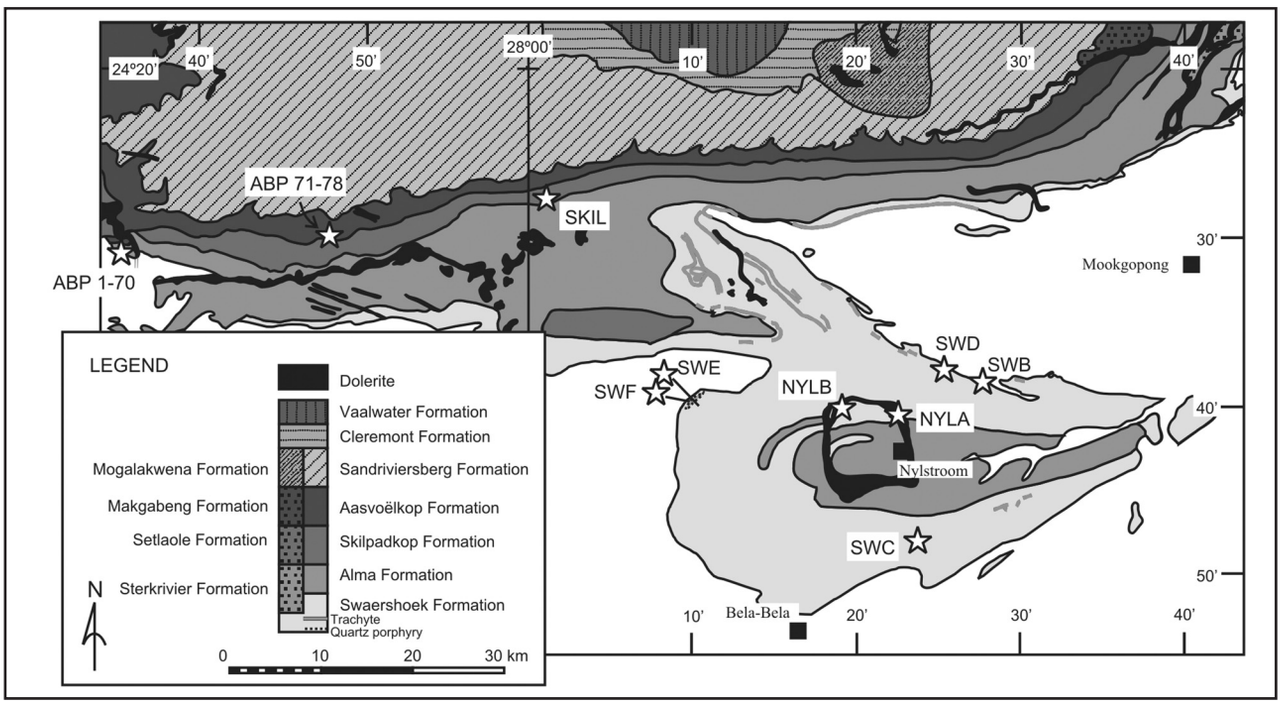

Figure 2. Geology of the Waterberg Group in the Nylstroom area, after Jansen (1982). Sampling localities are indicated.

sun compass as well. Cores were trimmed to 2.4-cm-long specimens and measured on 2G-Enterprises ™ SQuID magnetometers housed at the University of Western Australia and at the California Institute of Technology. Demagnetization steps varied among the localities and lithologies studied, but generally consisted of about 15 steps. A demagnetization sequence typically started with a measurement of natural remanent magnetization (NRM) followed by a stepwise low-field-strength alternating-field pretreatment in five successive steps up to 10 mT. Samples were then thermally demagnetized in a shielded furnace at decreasing intervals until specimen intensity dropped below noise level. Magnetic components were identified and quantified via least-squares principal-component analysis (Kirschvink, 1980). These calculations, together with all subsequent statistical analyses, utilized the Macintosh™ based computer programmes Paleomag 3 (Jones, 2002) and PaleoMac (Cogné, 2003). All calculations of paleomagnetic poles assume an axial-geocentric dipolar geomagnetic field and a paleoradius for the Earth equal to the present Earth radius.

Results

The results of least squares analysis for all the sampling sites and a summary of stability field tests for the high temperature components are provided in Tables 1 and 2, respectively.

Swaershoek Formation

SWF (Quartz porphyry and fine red quartzite and shale)
Locality SWF is situated on the farm Rhenosterpoort (S 24°39'23.9" E 028°10'25.6") ~25 km west of Nylstroom (Figure 2). A quartz porphyry near the base of the stratigraphic section here (Figure 3) gave a Pb^{207}/Pb^{206} zircon SHRIMP age of 2054.1 ± 3.5 Ma (Dorland *et al.*, 2006). Samples of the porphyry as well as associated sedimentary rocks (mostly brick-red shale, but also quartzite and rare banded-chert) were collected from eight decameter-scale sampling intervals (SWF-A to H).

Site SWF-A represents folded red shale as well as consistently eastward dipping sedimentary rocks that directly overlie the folded strata along a faulted contact. This site is stratigraphically just below the quartz porphyry. About 100 m south along strike of the consistently dipping shale of site SWF-A, more shale with interfingered quartz porphyry was sampled (site SWF-B). The same quartz porphyry unit was sampled at site SWF-C, ~15 m northeast of SWF-B. Forty-seven meters above the dated quartz porphyry, quartzite is followed by conglomerate with slab-like clasts of red shale. Two samples (SWF 26 and 27) were drilled from the quartzite and were included with site SWF-C. Five shale clasts were sampled for a conglomerate test together with the matrix of the conglomerate and overlying purplish sandstone to provide another site (SWF-D). Site SWF-E (330 m southeast and stratigraphically above site SWF-D) provides another conglomerate test. Here clasts of both red shale and quartz porphyry were collected. Sample site SWF-F returns to the quartz porphyry at the base of the section (in proximity of sites SWF-A, B and C). Here, sampled rocks include quartz porphyry as well as a 1 m-thick banded-chert layer, which occur ~75 m stratigraphically below the porphyry. Folded red shale, roughly at the same stratigraphic position as the folded strata of site SWF-A, provided for another fold test (SWF-H).

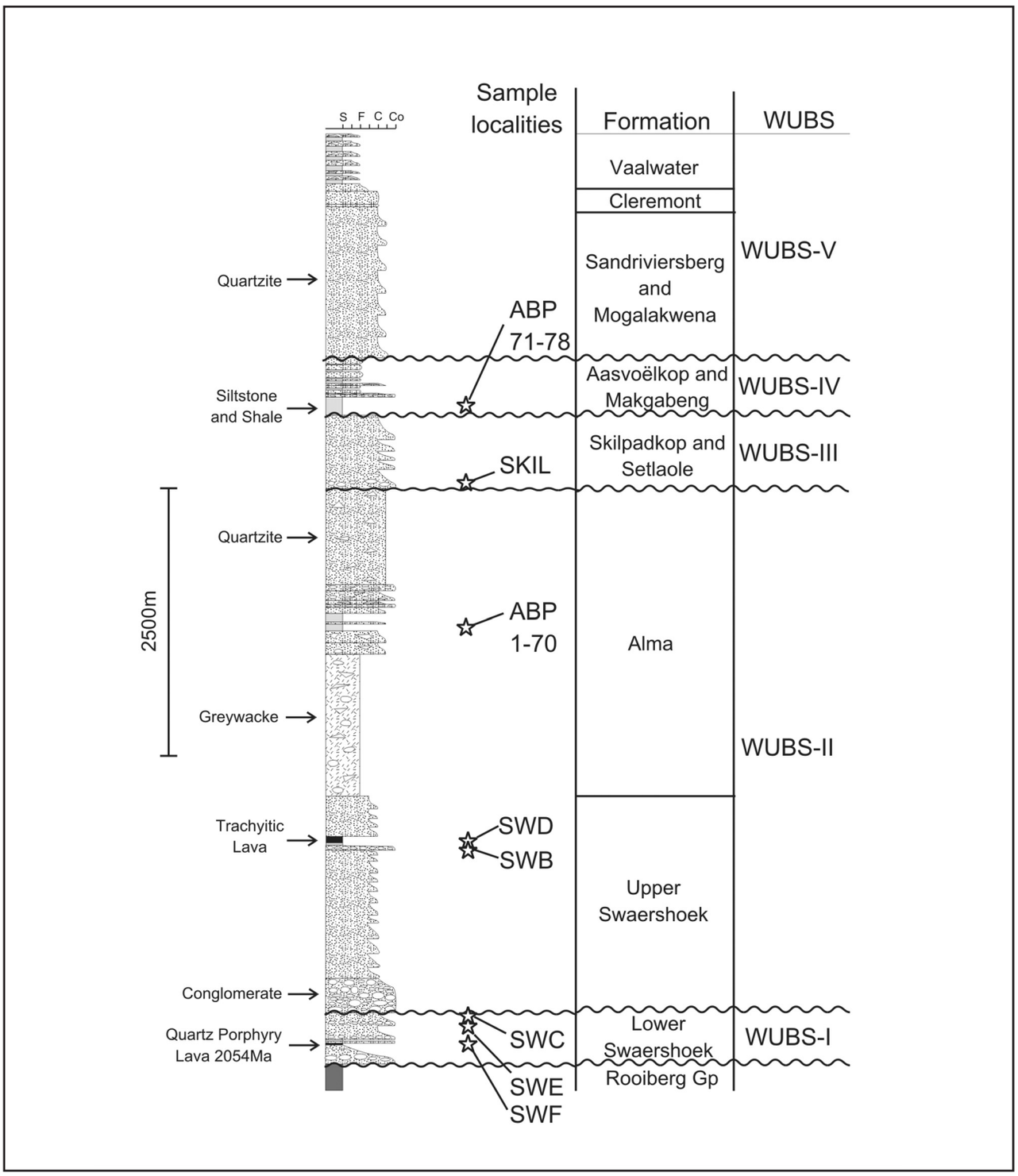

Figure 3. Stratigraphic setting of sampling localities and of the ~2.05 Ga quartz porphyry lava (Dorland *et al.*, 2006) from near the base of the Waterberg Group.

The samples from the different sampling sites (and lithologies) displayed similar behavior during demagnetization and are summarized here, while a more detailed description for the sites that provided field tests follows in the next paragraph. Four magnetic components were identified during principal-component analyses. Each sample typically recorded at least three out of four magnetic components identified among the entire sample suite (Figures 4 and 5a-h). The first component was removed through AF pretreatment and thermal steps generally below 550°C. Site SWF-G (Figure 5g) is an exception, as this component remains stable up to 680°C and is recorded as a sole component by most samples from this site. The component (abbreviated LOW) is oriented upwards and northerly in geographic coordinates and although site means are not well defined, grouping (k) generally worsens when bedding is restored to zero. A westerly and down-

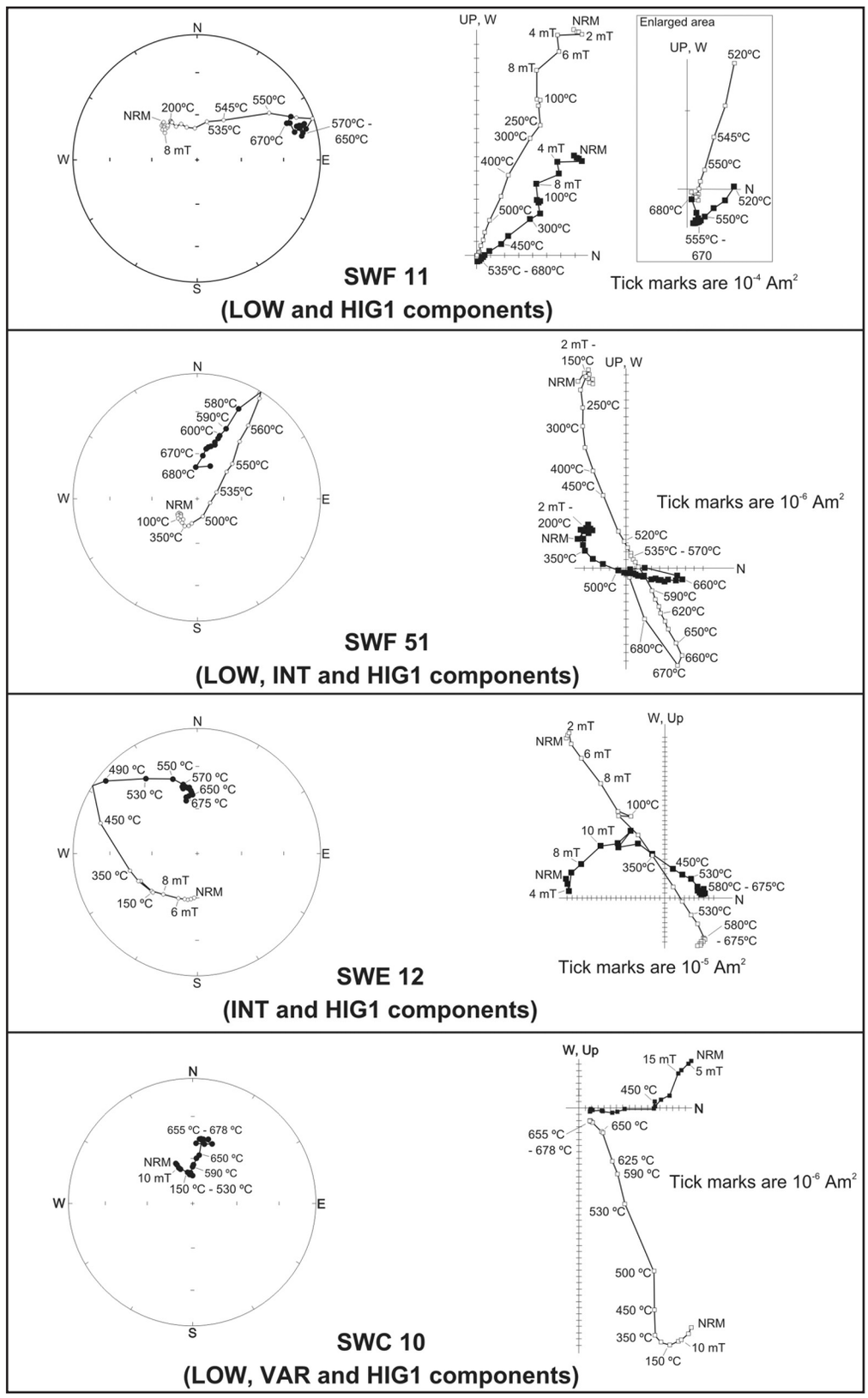

Figure 4. Representative sample demagnetization behavior, in situ field coordinates, from quartz porphyry lava and brick-red shale from localities SWF and SWE in the lower part of the Swaershoek Formation. Orthogonal projection plots: solid = horizontal plane, open = north-south and vertical plane. Equal-area projection plots: solid = lower hemisphere, open = upper hemisphere. NRM = natural remnant magnetization.

directed component (abbreviated VAR) is present at five of the sampling sites. It is revealed by low thermal demagnetization steps or by the AF pretreatment steps in some samples, but persists up to 680°C in others. This component displays much more variability in unblocking than any of the other components. In contrast to this variability, a clear intermediate temperature component (that generally unblocks below 600°C) was revealed in 34 samples. This third component is directed upwards in a south-southwesterly direction (abbreviated INT). At high levels of demagnetization (above 600°C) a fourth component was revealed either as stable end-points of demagnetization trajectories or as great circle arcs towards a northeasterly and down direction (abbreviated HIG1). In relatively rare instances where both line and plane data were obtained they were analyzed together as unit-weighted lines and half-weighted, restricted planes (McFadden and McElhinny, 1988).

At sampling site SWF-A eleven samples were collected for a fold-test (Figure 5a and 6a). Brick-red shale is folded about a southwesterly plunging fold axis. Folding was followed by one or more episodes of brittle deformation that not only duplicated the southwest plunging fold but also juxtaposed it against uniformly southeasterly dipping shale. Bedding data from the sampling site define a cylindrical best-fit fold axis that plunges steeply (~65°) to the southwest. Although a success rate of ~50% for isolating the HIG1 component in red shale was achieved, which is typical when compared to the success rate achieved at other sites (see Table 1), it is, however, unfortunate that the six samples that did work are from similarly dipping beds. Grouping does improve after a structural correction is applied to the data (Figure 5a). Statistically, however, the ratio of the groupings of these linear components in geographic and tilt-corrected coordinates is inconclusive at inferring either a positive or negative kappa-ratio (KR for short) fold test or modified form of Graham's fold test as described by McElhinny (1964). Although it has been pointed out by McFadden and Jones (1981) that the criterion on which this test is based is statistically invalid, it is nonetheless a conservative measure in practice. The statistically more sound fold tests of McFadden (1990) and the so-called "DC fold test" of Enkin (2003) yield equally ambiguous, but not demonstrably negative, results. The result of the DC fold test (Figure 6a) suggests that the bedding attitudes of samples are not significantly different from one another to illustrate a successful fold test.

At site SWF-H samples were collected for another fold test (Figure 5h and 6b). A cylindrical best fit for the bedding data results in a fold axis that plunges moderately to the southwest (247.4°/24.5°). Six out of eleven samples yielded a high-temperature component. These samples were more evenly distributed around the fold axis than the samples from site SWF-A. Once again the KR fold test result is inconclusive, but in this case the McFadden (1990) fold test and the DC fold test are positive. The best result is achieved at 84.0% ± 18.9% unfolding at 95% confidence, which is not significantly different than 100% unfolding (Figure 6b). This suggests that the HIG1 remanence is pre-folding in origin. The ambiguous KR fold test is not surprising since it has been pointed out that statistically this test is prone to fail when bedding variations are small relative to paleomagnetic dispersion (Enkin, 2003).

The question arises as to whether the folding records deformation of lithified rock or unlithified sediment. Soft-sediment deformation could either reflect syn-sedimentary tectonism or sediment disturbance by other mechanisms. However, if the folds were soft-sediment in origin a syn- or post-folding age (and not a pre-folding age) would be expected for the most common types of remanence acquisition. Concerning the extent of deformation, the brick-red shale and sandstone that directly overlie the porphyry appear not to be folded, but beds at one of the sampling sites (SWF-B) are slightly deformed about a similar moderately plunging southwesterly axis. A structural correction (same plunge correction as for SWF-H) was applied to site SWF-B. No plunge correction was applied to the remainder of the sites.

Five samples (SWF 28-33, with the exception of 31, which is representative of the matrix) were drilled from shale clasts for a conglomerate test and an additional eight samples were collected from overlying purplish sandstone (site SWF-D). The clasts and sandstone samples from site SWF-D typically displayed two to three magnetic components each. The components removed at lower demagnetization levels were either the LOW or INT components as discussed earlier. The groupings (k) of these components worsen dramatically (Figure 5d) when the clasts and sandstone are restored to horizontal. Restoration of clasts to horizontal was done by tilt-correcting bedding attitudes obtained directly from the clasts or by using clast oblateness as a measure of how much clasts have been tilted. Based on their non-random distributions in geographic coordinates, the LOW and INT components are interpreted to post-date deposition of the conglomerate. High temperature components were only plotted for those clasts that recorded magnetic histories consistent with underlying Swaershoek samples (samples 28, 30 and 32). These high-coercivity directions are distributed at random (Watson, 1956) in geographic coordinates (Figure 5d). When the clasts are restored to horizontal these components plot along the same narrow small circle of inclination (47.2° ± 7.7°; Figure 5d). This inclination is consistent with the inclination of the HIG1 components as revealed in the underlying Swaershoek samples. This can be expected for a primary remanence recorded in clasts that have been tilted, rotated about a vertical axis or been overturned due to current action during deposition. Note, however, that high-coercivity (HIG1) components were only identified in two of the sandstone samples (sample 34 and 41). This low success rate together with

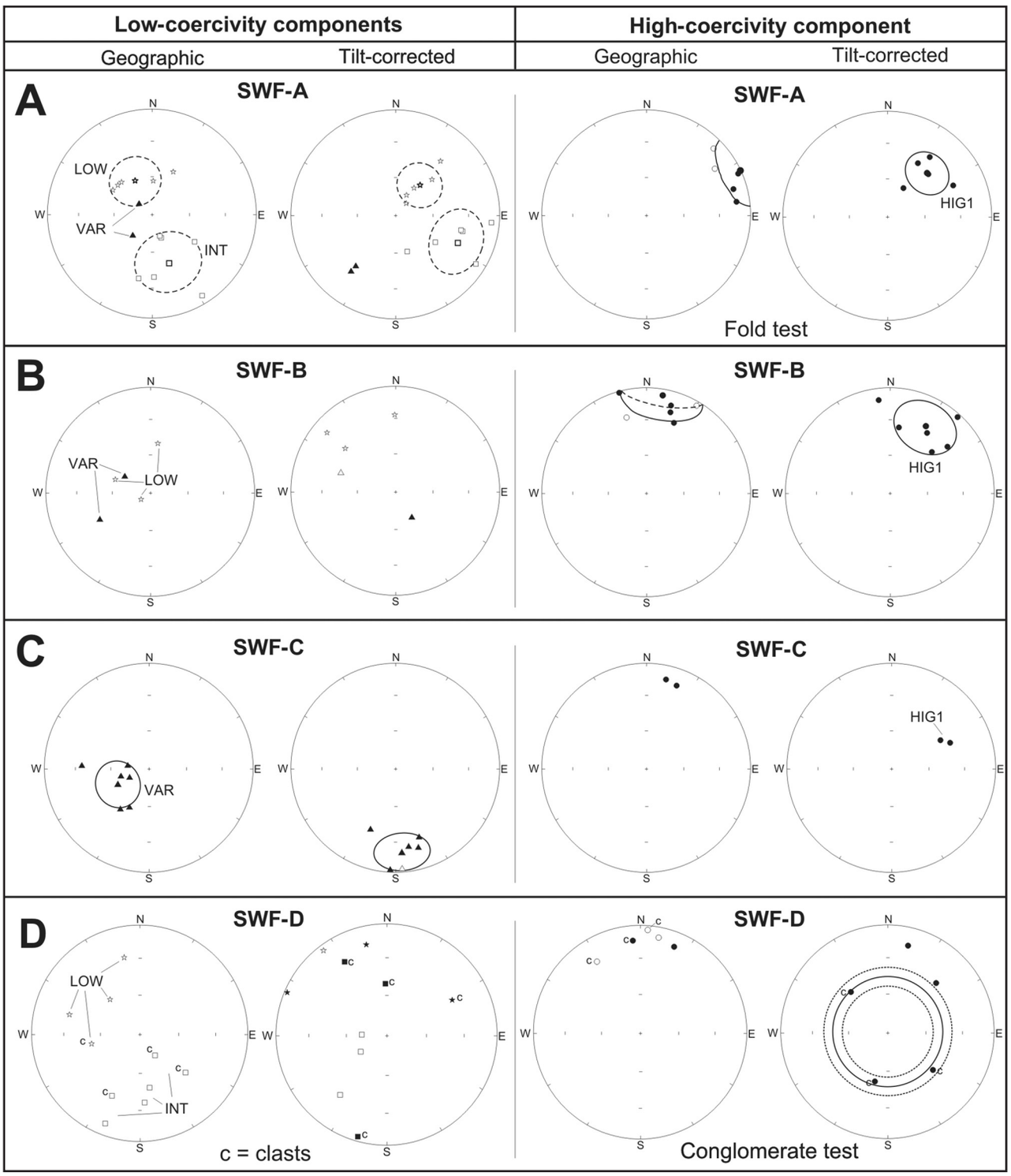

Figure 5. Equal area plots of results from the SWF locality. The left-hand panel depicts low-coercivity components in geographic and tilt-corrected coordinates, while the right-hand panel depicts the high-coercivity component. (**A** and **H**) are fold tests from sites SWF-A and H and (**D** and **E**) are conglomerate tests from site SWF-D and E. Open symbols indicate negative inclinations (upward directed components) and closed symbols are positive inclinations or downward directed components. Star = LOW components, Square = INT components, Upward Triangles = VAR components, and Circle = HIG1 components.

the substantial amount of scatter shown by the lower coercivity components from clasts and the sandstone at this site is discouraging. For these reasons the conglomerate test at site SWD is regarded as inconclusive (neither negative or positive).

Another sampling site (SWF-E) situated in a small stream gully, well away from site SWF-D was sampled for an additional conglomerate test. This conglomerate marks the base of Waterberg unconformity-bounded sequence II in our interpretation (see Dorland *et al.*,

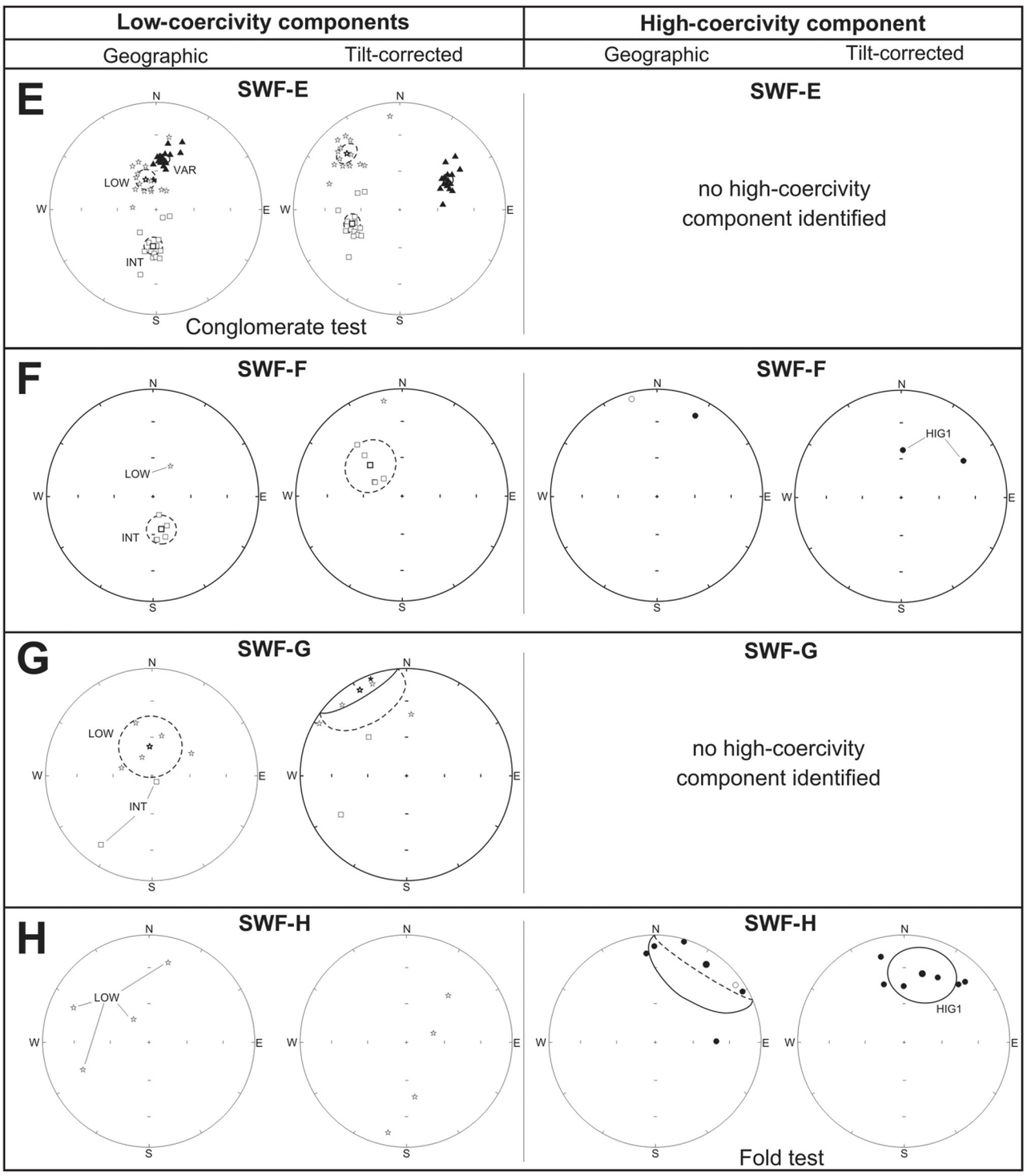

Figure 5. Equal area plots of results from the SWF locality. The left-hand panel depicts low-coercivity components in geographic and tilt-corrected coordinates, while the right-hand panel depicts the high-coercivity component. (**A** and **H**) are fold tests from sites SWF-**A** and **H** and (**D** and **E**) are conglomerate tests from site SWF-**D** and **E**. Open symbols indicate negative inclinations (upward directed components) and closed symbols are positive inclinations or downward directed components. Star = LOW components, Square = INT components, Upward Triangles = VAR components, and Circle = HIG1 components.

2006). Both porphyry and mudstone clasts were sampled and rare examples of both clast lithologies displayed 'liesegang' banding truncated by the clast edges, suggesting preservation of hematitic weathering from prior to conglomerate deposition. In most cases each clast recorded three magnetic components: a LOW component, an INT component and a northerly-down component with generally high unblocking temperatures, which we have labeled "VAR". All three components displayed good groupings (k = 24, 38 and 73 respectively) in geographic coordinates, suggesting that these remanence directions post-date conglomerate

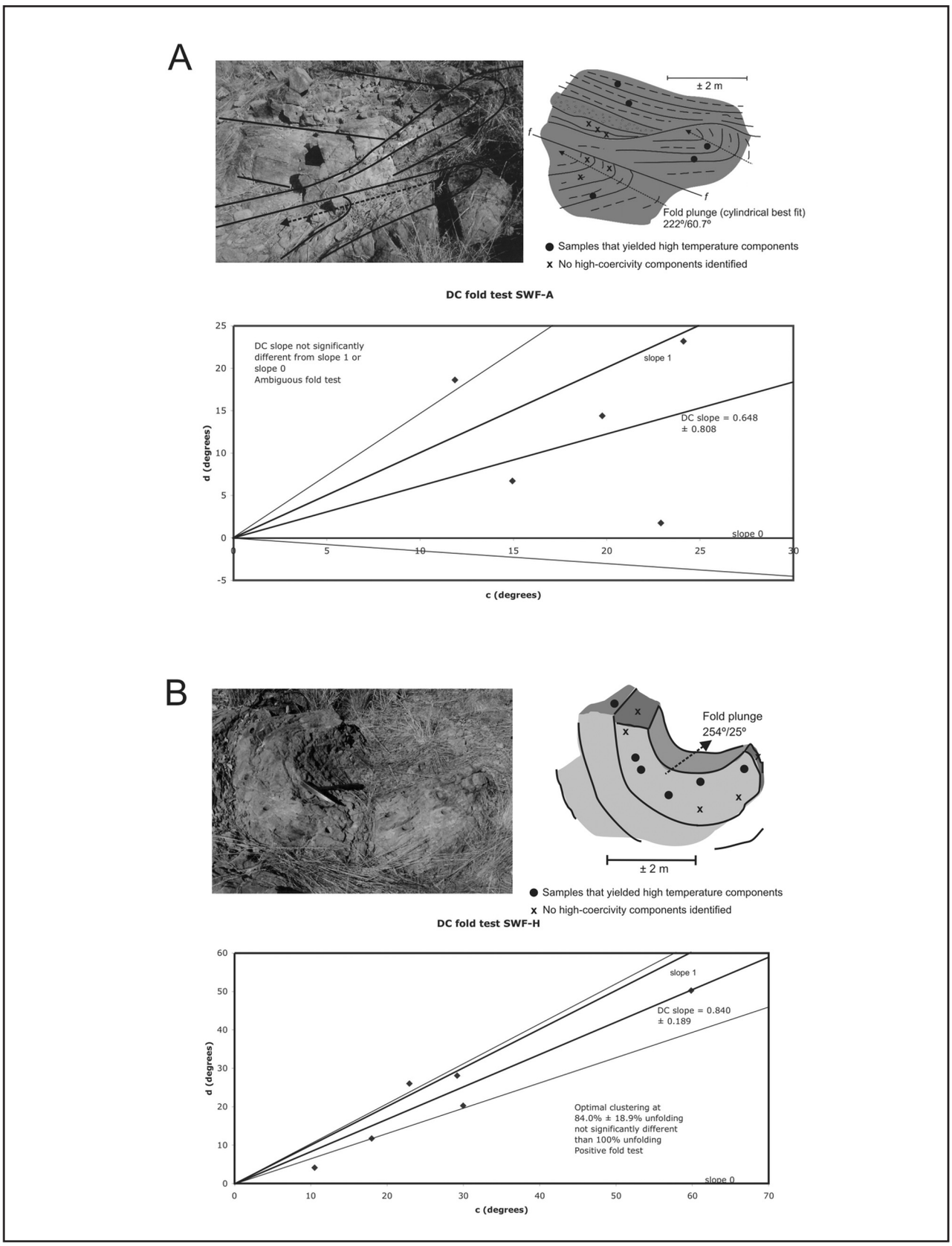

Figure 6. (**A**) Fold test at site SWF-A. Field photograph, looking west, of the SWF-A fold test site. Structure is enhanced digitally. Right-hand panel shows a field sketch of the structure with sample positions. Summary of DC-fold test (see Enkin (2003) for definitions of (**C** and **D**) is also shown). The DC plot shows how the DC slope is not significantly different from either 1 or 0, resulting in an indeterminate fold test. The test is not demonstrably positive or negative. (**B**) Fold test at site SWF-H depicted in a similar fashion. The DC-plot shows how the DC-slope is not significantly different from 1, but it is significantly different from 0, indicating the remanence to be pre-folding in age.

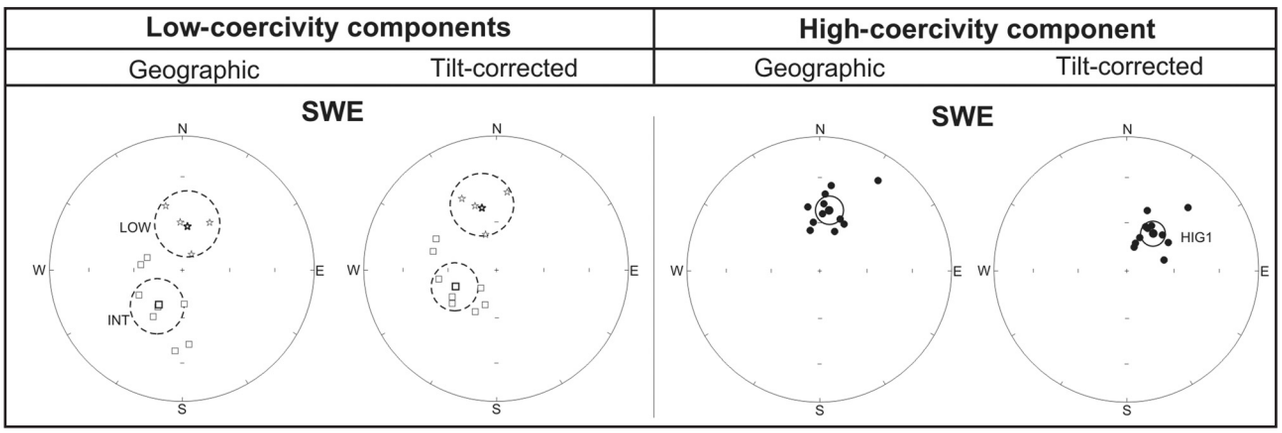

Figure 7. Equal area plots of results from locality SWE. Symbols are as for Figure 5.

deposition (Figure 5e). Each of these three directions is therefore a magnetic overprint.

It must be stated that distinguishing between the northerly VAR directions as recorded at some of the sites and the exclusively high-temperature northeasterly HIG1 components can be quite difficult depending on bedding orientations. A cursory consideration of the negative conglomerate test on northerly-down component VAR might suggest that HIG1, too, is a magnetic overprint, postdating sedimentation of Waterberg unconformity-bounded sequence II. However, we maintain that this is not the case, because of the positive fold test elsewhere in the section as noted above. We suggest instead that localized hydrothermal fluids overprinted the SWF-E site, either immediately after conglomerate deposition or at a time when the Kaapvaal APWP returned to a position similar to that at ~2.05 Ga. A potential candidate time for such local overprinting is ~ 1.88 Ga, when post-Waterberg diabase extensively intruded the basin and imparted paleomagnetic directions similar to the VAR component at this site (see Hanson *et al.*, 2004a).

SWE (Fine red quartzite and shale)

A profile (site SWE, Figure 3), located ~475 m stratigraphically above the SWF-E sampling site, was sampled in the so-called "Lower" Swaershoek sedimentary rocks. The locality (S 24°39'35.8", E 028°10'59.7") was reached from the western end of the farm Zuurvlei. A total of 19 samples were collected over a stratigraphic thickness of about 300 m from the reddish quartzite that crops out at this sampling locality.

An overview of the data reveals three magnetic components and demagnetization behavior very much akin to that observed at locality SWF (Figures 4, 7). Demagnetization through AF pretreatment and thermally up to 570°C shows the unblocking of a similar LOW direction as recorded in SWF samples. At intermediate demagnetization temperatures (below 600°C) the second component unblocks in a southwesterly downward direction (INT). The third component was revealed at high demagnetization levels (above 600°C) either as stable end-points of each sample's demagnetization trajectory or as great circle arcs away from the INT direction. This high-coercivity component is oriented northerly and down and very similar to the primary HIG1 direction revealed during high demagnetization levels at locality SWF (Figure 5). The HIG1 component was identified in 10 out of the 19 samples collected from this locality.

SWC (Fine red quartzite and shale)

Two sampling sites (100 m apart) and a total of 14 samples were collected from a road cut (S 24°46'47.8", E 028°24'37.61"), which is stratigraphically similar to site SWF-E (Figure 3). Samples were collected from uniformly shallowly dipping fine-grained quartzite interbedded with shaly layers (SWC-A) and from a massive fine-grained quartzite (SWC-B, ~10 m stratigraphically above SWC-A). Samples from both sampling sites displayed identical behavior during demagnetization (Figure 8a and b). Three magnetic components similar to those discussed above were identified. The first component is removed through AF pretreatment and thermal demagnetization generally below 350°C and is directed parallel to the LOW components seen at the other localities. A steep downward, northwesterly (VAR) component was removed next in the temperature range 350°C to 550°C. At high levels of demagnetization (above 600°C) a less steep, downward northerly direction was removed (similar to the high-coercivity HIG1 components from SWF, see Figure 5).

SWB (Red shale)

Stratigraphically above the localities described thus far and situated along the northern limb of the Nylstroom syncline, 21 samples were collected at locality SWB (S 24°38'38.9", E 028°29'19.7") from steeply dipping shale that crops out along a dirt road on the farm Groenfontein 383. Samples were collected over a stratigraphic thickness of 57 meters (Figure 3).

Sample behavior during demagnetization is quite distinct from that discussed earlier (Figure 9 and 10). Firstly: the LOW component is preserved in only six samples and is thus much more poorly developed than

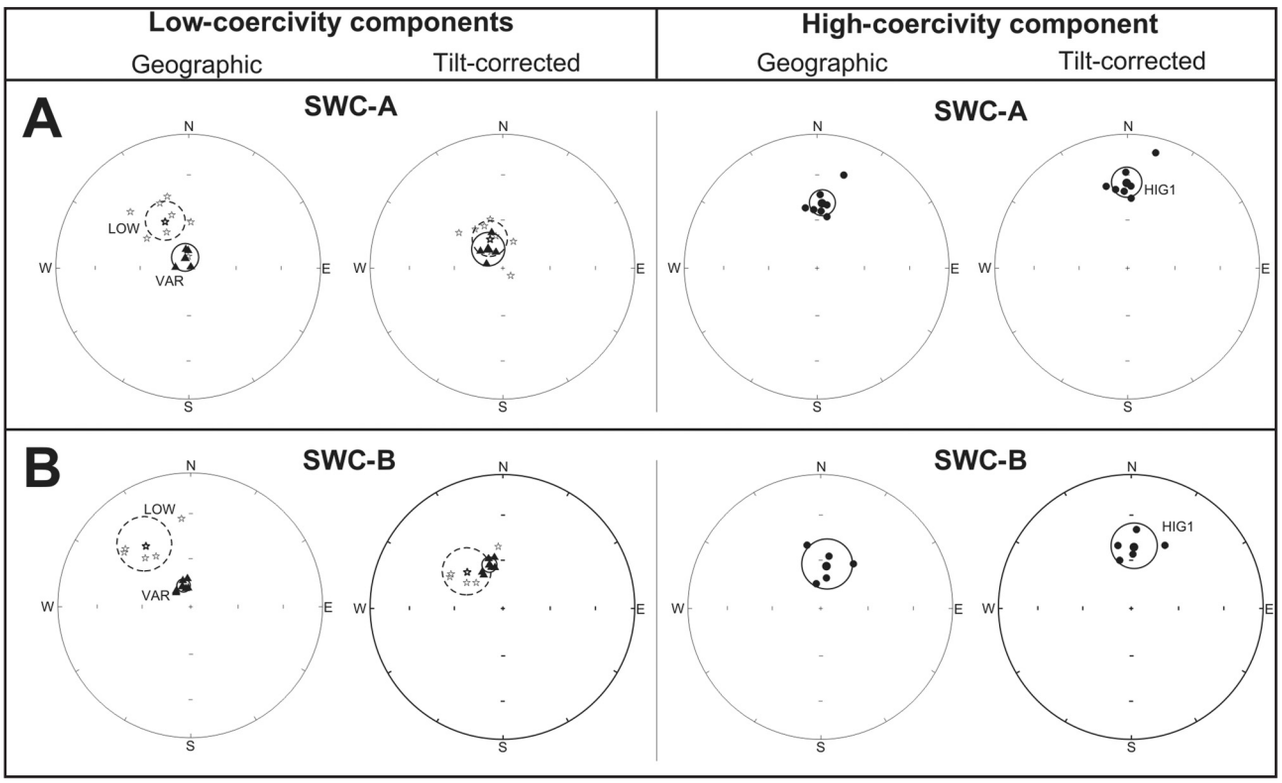

Figure 8. Equal area plots of results from locality SWC. Symbols are as for Figure 5.

at other localities; yet the stratigraphically lowest of these six samples recorded it as a sole component. Second, only two samples recorded the INT remanence component (below 630°C). Third, apart from the stratigraphically lowest samples (SWB 1-8) that appear to be heavily affected by the LOW overprint, or that display behavior that is too noisy for any interpretation to be made, most samples (11 out of 21) recorded a dual-polarity component directed west and down (HIG2-) or east and up (HIG2+) through AF pretreatment and thermal demagnetization steps below 650°C (but sometimes persisting up to 670°C). The HIG2- component is easily distinguished from the VAR component, in that the HIG2- component is less steep (~36° compared to the 69° average inclination of the VAR component from other localities in geographic coordinates), and the VAR component is directed more northerly. Considering the HIG2 components, the sampling site records two stratigraphically constrained polarity groups. Unfortunately, a reversals test (McFadden and McElhinny, 1990) gives an indeterminate outcome (Table 2), but this is due to the low number and relative poor grouping (n = 4; k = 12.59) of the HIG2- vector directions compared to the HIG2+ directions (n = 7; k = 16.09). The presence of two polarities is nonetheless supportive of a primary remanence.

SWD (Trachytic lava)

In a relatively continuous stream exposure (S 24°37'42.2", E 028°25'25.1") five km to the northwest and along strike from site SWB on the farm Buffelshoek 384, six individual trachytic lavas were sampled. Each flow was sampled at a site (SWD-A to F) and provided 5 to 6 core samples. SWD-A represents the lowermost exposed lava flow. Only the uppermost part of this massive lava flow is exposed. A brecciated flow top or breccia flow (~2 m thick) provided 6 samples for a potential conglomerate test (SWD-B). Immediately above this breccia flow an 18 m thick amygdaloidal lava flow was sampled (SWD-C), despite its weathered appearance. Site SWD-D constitutes an exposed amygdaloidal flow-top occurring 15 m stratigraphically above site SWD-C. Another amygdaloidal flow-top (site SWF-E) is exposed approximately 15m downstream (upsection) from SWD-D. The top-most exposed lava flow (SWD-F) is characterized by prominent flow banding and possible pillow textures towards the top. This flow is ~50 m stratigraphically above the first lava exposure.

Three magnetic components were identified through principal-component analyses of demagnetization data (Figures 11a to f). Each sample typically recorded only two of these. Through AF pretreatment and thermal demagnetization, generally below 250°C, the LOW component was revealed in most of the samples from all the sites. In some samples that originate from sites SWD-E and F (upper two lava flows) this component persisted to very high levels of demagnetization or even existed as a single component that remained stable up to 600°C. A few samples (mostly from site SWD-B, but also from SWD-E and F) recorded the INT component (Figure 11b, e and f). This component was revealed either through AF pretreatment and low thermal steps or demagnetization in the temperature range 250 to 550°C.

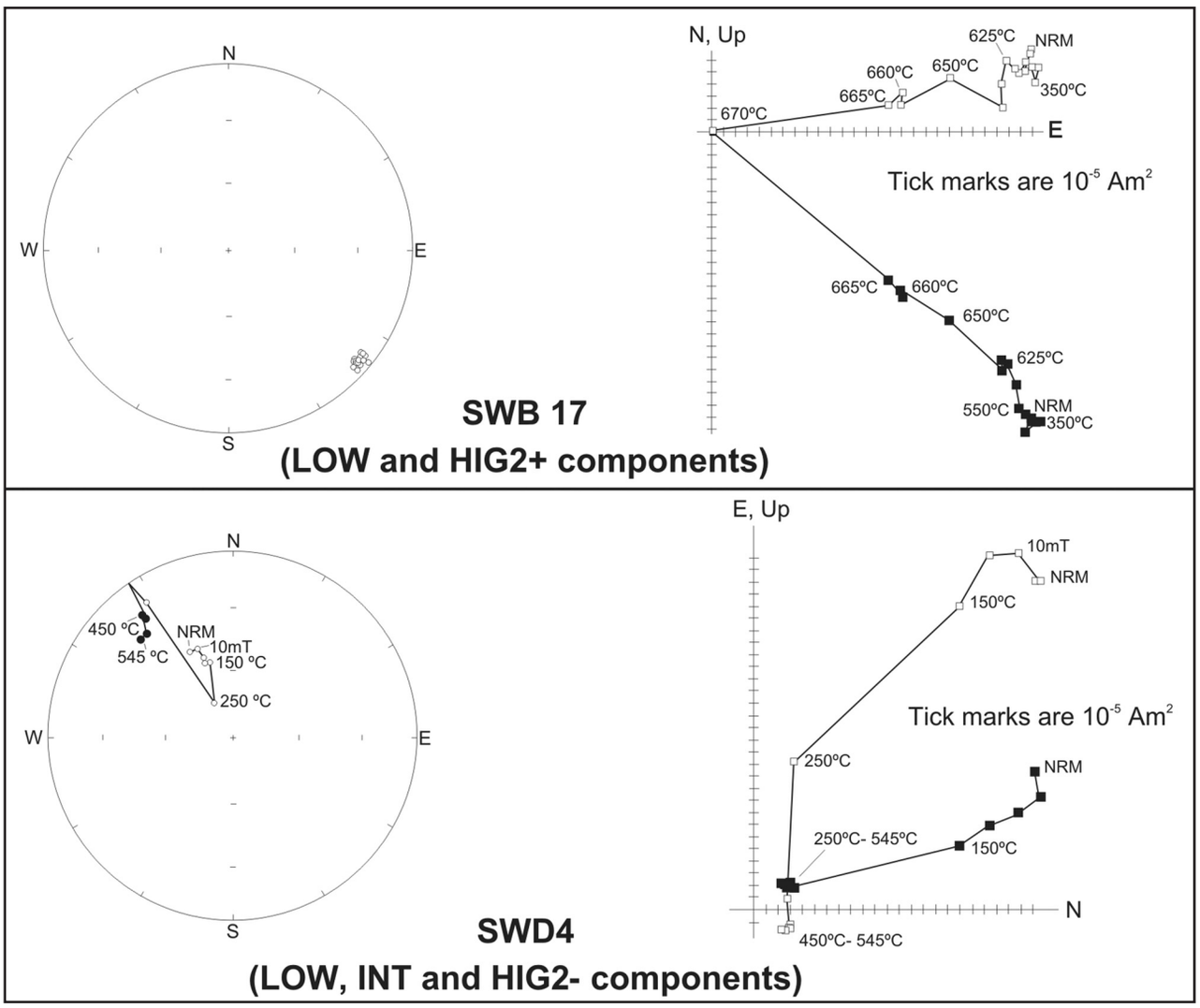

Figure 9. Representative sample demagnetization behavior, in situ field coordinates, from shale and trachyitic lava from localities SWB and SWD in the upper part of the Swaershoek Formation. Symbols are as in Figure 4.

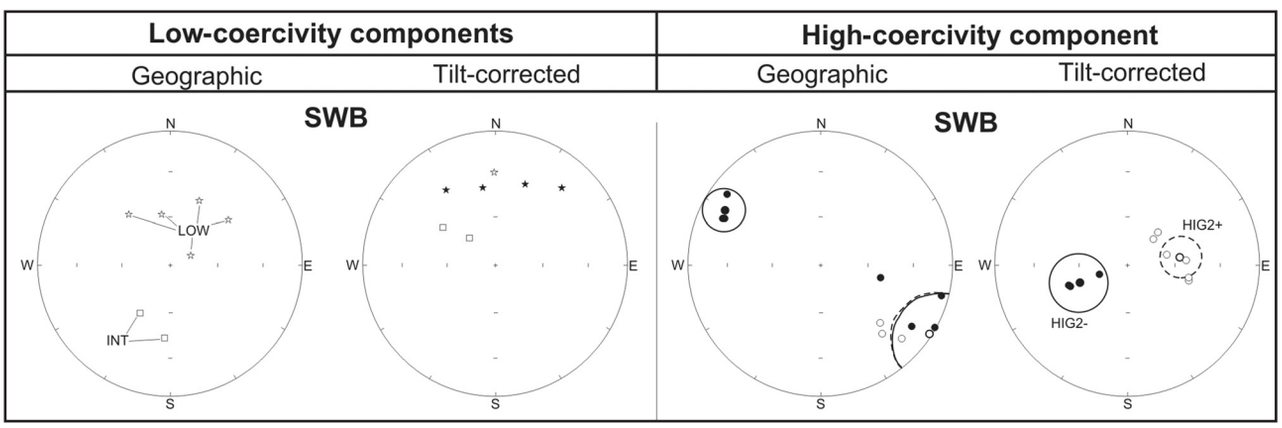

Figure 10. Equal area plots of results from locality SWB. Symbols are all as for Figure 5, except that Circle = HIG2-/+ components.

An additional component was present in most of the samples from the lower flows (Figures 11a to d), but was only identified in three samples from the upper two flows (Figures 11e and f). This westerly and down component unblocked in the temperature range 350 to 600°C and resembles the high stability HIG2-component revealed in samples from site SWB (Figure 10).

Clasts from a blocky lava flow (site SWD-B) were sampled with the intention to do a conglomerate test. However, the revealed high-coercivity components clearly fail the test (Figure 11b, Table 2). The calculated

Table 1. Summary of Least Squares Component Directions for the Swaershoek and Alma Formations and post-Waterberg intrusions[a]

		Present coordinate			Tilt-corrected coordinates							
Component												
Site	**Lithology**	**n/N**	**L/P**	**T_{unbl} in °C**	**D in deg.**	**I in deg.**	**k**	**a_{95} in deg.**	**D in deg.**	**I in deg.**	**k**	**a_{95} in deg**
Secondary												
LOW												
SWF-A	shale	5/11	L	<150	**333.1**	**-60.8**	**12.73**	**19.78**	63.4	-59.8	15.71	17.7
SWF-B	sh., porph.	3/9	L	<550	323.9	-71.9	5.83	44.48	317.6	-27.0	4.64	45.81
SWF-D	shale clasts, qzt.	4/14	L	<200	305.7	-48.0	6.90	37.80	338.2	16.8	2.50	74.60
SWF-E	sh., porph. clasts	15/25	L	<400	**339.7**	**-65.4**	**24.18**	**7.66**	**316.5**	-27.8	24.18	7.65
SWF-F	porphyry	2/6	L	AF or <550	345.8	-41.9	–	–	341.6	22.1	–	–
SWF-G	sh., chert	5/7	L	<680	345.1	-62.6	4.98	31.93	328.6	-5.1	4.81	32.60
SWF-H	shale	4/11	L	AF or <550	311.1	-50.7	2.87	51.09	156.9	-64.8	1.99	66.45
SWE	quartzite	5/18	L	<570	338.6	-67.6	6.31	29.06	326.4	-43.9	6.39	28.85
SWC-A	quartzite	6/8	L	<450	**328.1**	**-42.0**	**21.24**	**13.53**	**330.9**	-56.1	28.79	11.56
SWC-B	quartzite	5/6	L	<250	**322.9**	**-30.9**	**15.85**	**17.62**	**315.5**	-48.2	15.23	17.99
SWB	shale	6/21	L	<250 or <670	33.8	-47.0	7.85	23.02	17.2	12.8	6.66	25.25
SWD-A	trachyitic lava	4/6	L	<450	351.6	-41.4	10.69	25.21	352.3	-2.4	10.86	25.00
SWD-B	trachyitic lava	6/6	L	<450	**326.7**	**-80.6**	**19.50**	**14.14**	348.5	-42.5	19.47	14.15
SWD-C	trachyitic lava	3/6	L	<350	347.5	-64.4	9.74	33.49	351.2	-25.4	10.05	32.94
SWD-D	trachyitic lava	3/6	L	<350	331.3	-47.5	50.47	14.27	340.6	-11.8	55.12	13.64
SWD-E	trachyitic lava	4/6	L	<350	295.3	-61.3	8.57	28.41	334.4	-36.9	8.57	28.42
SWD-F	trachyitic lava	2/6	L	<350	58.7	-84.4	–	–	15.9	-47.1	–	–
ABP 1-65	shale	47/65	L	generally <450	**316.2**	**-61.3**	**16.16**	**5.34**	315.1	-64.3	15.93	5.38
ABP 66-70	dolerite	5/5	L	<450	**339.9**	**-33.4**	**62.71**	**8.70**	339.9	-33.4	62.71	8.70
ABP 71-78	sh., qzt.	3/8	L	<500	28.3	-64.9	9.80	33.38	36.9	-67.8	16.83	25.06
SKIL	shale clasts	11/14	L	<500	**334.5**	**-55.8**	**10.16**	**14.29**	324.9	-70.0	10.20	14.26
VAR and VAR?												
SWF-A	shale	2/11	L	variable	254.6	76.8	–	–	-220.3	35.4	–	–
SWF-B	shale	2/9	L	variable	263.5	58.6	–	–	-189.3	57.4	–	–
SWF-C	porph., qzt.	6/7	L	variable	265.5	60.7	8.79	21.63	181.1	32.1	4.59	30.38
SWF-E[b]	sh., porph. clasts	17/25	L	variable	**8.3**	**50.2**	**73.35**	**4.16**	58.6	45.8	74.29	4.17
SWF-H	shale	4/11	L	variable	197.0	77.6	27.69	15.32	198.8	58.7	8.43	28.67
SWC-A	quartzite	4/8	L	<550	356.5	88.6	29.00	14.96	316.2	76.0	10.37	25.63
SWC-B[b]	quartzite	6/6	L	<550	**339.2**	**71.5**	**131.17**	**5.36**	342.4	52.0	118.99	5.63
ABP1-65	shale	12/65	L	<650	320.7	28.9	12.37	12.26	320.5	24.7	11.97	12.48
INT												
SWF-A	shale	6/11	L	<550	**161.2**	**-49.2**	**6.87**	**24.81**	131.6	-34.9	9.82	20.36
SWF-D	shale clasts, qz.	6/14	L	<600	**176.2**	**-44.5**	**6.99**	**24.57**	259.3	-80.2	3.00	39.78
SWF-E	sh., porp. clasts	13/25	L	<630	**185.0**	**-59.4**	**38.45**	**6.50**	250.6	-50.7	38.56	6.49
SWF-F	porphyry	5/6	L	<600	**165.3**	**-67.3**	**21.54**	**15.01**	315.7	-51.0	11.85	20.55
SWF-G	chert	2/7	L	<680	222.8	-30.2	–	–	250.1	-26.0	–	–
SWF-H	shale	2/11	L	<620	169.1	-49.1	–	–	154.5	2.7	–	–
SWE	quartzite	7/18	L	<550	189.3	-52.8	3.91	30.94	236.8	-65.2	5.23	26.58
SWB	shale	2/21	L	<635	155.9	-40.3	–	–	0.8	-59.6	–	–
SWD-B	trachyitic lava	2/6	L	<570	146.0	-50.9	–	–	73.6	-72.3	–	–
SWD-E	trachyitic lava	2/6	L	<570	163.3	-38.3	–	–	-123.7	-67.5	–	–
SWD-F	trachyitic lava	2/6	L	<570	240.5	-68.3	–	–	-334.3	-60.4	–	–
ABP1-65	shale	35/65	L+P[c], (34, 1)	<650	**175.8**	**-58.1**	**16.08**	**6.29**	173.9	-55.0	16.52	6.2
ABP 71-78	sh., qzt.	6/8	L	<650	155.5	-41.4	6.58	25.43	155.8	-32.7	25.41	–
SKIL	shale clasts	8/14	L	<625	**172.7**	**-50.1**	**92.25**	**5.42**	171.9	-35.0	91.73	5.44

[a]Abbreviations: n/N, number of samples included in mean/number analyzed; L/P, line versus plane least squares analysis (Kirschvink, 1980); T_{unbl}, unblocking temperature spectrum; D, mean declination; I, mean inclination; k, Fisher's (1953) precision parameter, except in modified form where lines and planes are combined (McFadden and McElhinny, 1988); a_{95}, radius of 95% confidence cone about mean; deg., degrees. Underlined and bold face means data were used to calculate paleomagnetic poles (Table 3).

[b]Data combined with post-Waterberg dolerite means reported by Hanson *et al.* (2004) for the calculation of a grand mean paleomagnetic pole.

[c]Combined line and half-weighted, restricted planes (McFadden and McElhinny, 1988)

[d]Corrected for plunge, 222.0°/60.7°, see text.

[e]Corrected for plunge, 247.4°/24.5°, see text.

Table 1. Summary of Least Squares Component Directions for the Swaershoek and Alma Formations and post-Waterberg intrusions[a]

		Present coordinate			Tilt-corrected coordinates							
Component												
Site	Lithology	n/N	L/P	T_{unbl} in °C	D in deg.	I in deg.	k	a_{95} in deg.	D in deg.	I in deg.	k	a_{95} in deg
Primary												
HIG1												
SWF-A[d]	shale	5/11	L+P, (3;2)	>570	64.7	0.0	11.97	20.44	**53.0**	**47.3**	**36.41**	**11.46**
SWF-B[e]	sh., porph.	6/9	L	>560	9.7	6.4	8.80	23.91	**19.1**	**29.0**	**9.65**	**22.72**
SWF-C	porphyry	2/7	L	>555	15.9	14.7	–	–	63.7	42.0	–	–
SWF-F	porphyry	2/6	L	>600	4.9	7.0	–	–	38.5	47.9	–	–
SWF-H[e]	shale	6/11	L	>600	33.0	13.4	3.68	34.80	**20.7**	**33.5**	**7.56**	**23.50**
SWE	quartzite	11/18	L+P, (6;5)	>570	9.2	42.2	18.70	10.31	**36.2**	**52.8**	**21.13**	**9.67**
SWC-A	quartzite	7/8	L	>500	5.2	39.3	37.58	9.22	**359.7**	**24.7**	**37.58**	**9.22**
SWC-B	quartzite	5/6	L+P, (4;1)	>560	12.5	56.7	24.05	17.30	**4.2**	**38.8**	**23.96**	**17.33**
HIG2+; HIG2-												
SWB	shale	11/21	L+P, (9;2)	AF or <650	121.7	-6.3	12.88	12.59	**75.6**	**-51.1**	**12.97**	**12.52**
SWD-A	trachyitic lava	6/6	L	>570	315.7	41.3	29.11	11.49	**269.3**	**61.9**	**28.99**	**11.52**
SWD-B	trachyitic lava	6/6	L	>450	291.3	43.3	14.98	16.24	**249.2**	**47.7**	**14.98**	**16.24**
SWD-C	trachyitic lava	4/6	L+P, (3;1)	>350	307.1	39.3	74.86	12.12	**265.3**	**55.4**	**74.34**	**12.16**
SWD-D	trachyitic lava	5/6	L	>350	315.5	38.0	19.68	17.68	**275.2**	**57.7**	**18.63**	**18.20**
SWD-E	trachyitic lava	1/6	L	>350	326.5	10.6	–	–	-313.0	36.5	–	–
SWD-F	trachyitic lava	2/6	L	>350	278.9	61.7	–	–	-230.1	42.8	–	–
ABP 1-65	shale	32/65	L+P, (31;1)	>625	85.0	-40.3	22.02	5.58	**87.3**	**-39.5**	**21.96**	**5.59**
ABP 71-78	sh., qzt.	3/8	L	AF or >650	112.7	-41.9	20.18	22.81	117.1	-37.8	20.37	22.70
DOL[b]												
ABP 66-70	dolerite	5/5	L+P, (4;1)	>450	**351.7**	**70.6**	**98.68**	**8.63**	–	–	–	–

[a]Abbreviations: n/N, number of samples included in mean/number analyzed; L/P, line versus plane least squares analysis (Kirschvink, 1980); T_{unbl}, unblocking temperature spectrum; D, mean declination; I, mean inclination; k, Fisher's (1953) precision parameter, except in modified form where lines and planes are combined (McFadden and McElhinny, 1988); a_{95}, radius of 95% confidence cone about mean; deg., degrees. Underlined and bold face means data were used to calculate paleomagnetic poles (Table 3).

[b]Data combined with post-Waterberg dolerite means reported by Hanson *et al.* (2004) for the calculation of a grand mean paleomagnetic pole.

[c]Combined line and half-weighted, restricted planes (McFadden and McElhinny, 1988)

[d]Corrected for plunge, 222.0°/60.7°, see text.

[e]Corrected for plunge, 247.4°/24.5°, see text.

average for the high temperature, westerly and down components approximates that of the overlying lava flow (SWD-C, Figure 11c) much closer than the average for the underlying massive flow. This might indicate some baking (and associated remagnetization) by the flow that immediately overlies the flow breccia. Another explanation for this apparently negative conglomerate test might be that the individual blocks sampled underwent only minor rotation. This might be a real possibility, if one considers within-site precision: the high-coercivity components for the underlying and the overlying flow (SWD-A and C) both have fairly good groupings (k = 29 and 74), as can be expected for a thermal-remanent magnetization recorded by an individual lava flow, yet the sampled flow-top blocks at SWD-B are characterized by a lower precision of k = 14 for the high-temperature component. We consider this conglomerate test inconclusive for these reasons.

Combining the least-squares results for the high temperature components (HIG2-) from locality SWD with that of SWB (which is only 5 km away geographically, but situated along strike) and reapplying the reversals test to the data results in a failed reversals test in geographic coordinates, but the data pass a "C" quality reversals test (McFadden and McElhinny, 1990) in tilt-corrected coordinates—due to a moderate change in dip between the two localities. This result may be considered as a two-polarity positive fold test, which, together with the stratabound nature of the reversal at site SWB, is a strong indication that the HIG2- and HIG2 + high temperature dual-polarity component represents a primary remanence.

Alma Formation

ABP (Purple shale and dolerite)

Shallowly dipping purple mudstone and shale were sampled from the drainage ditch beside the road ascending Bakker's Pass (S 24°29'24.0", E 027°33'36.0"). The section is ~40 m thick and crosses the lower contact of a prominent post-Waterberg sill that was dated by Hanson *et al.* (2004a) at 1872 ± 1 Ma. Shale and mudstone samples generally revealed three magnetic components during demagnetization (Figures 12 and 13a), namely the LOW component at low levels of demagnetization, the southerly-upward INT intermediate temperature component and an east-upward HIG2+ component at higher levels of demagnetization (similar

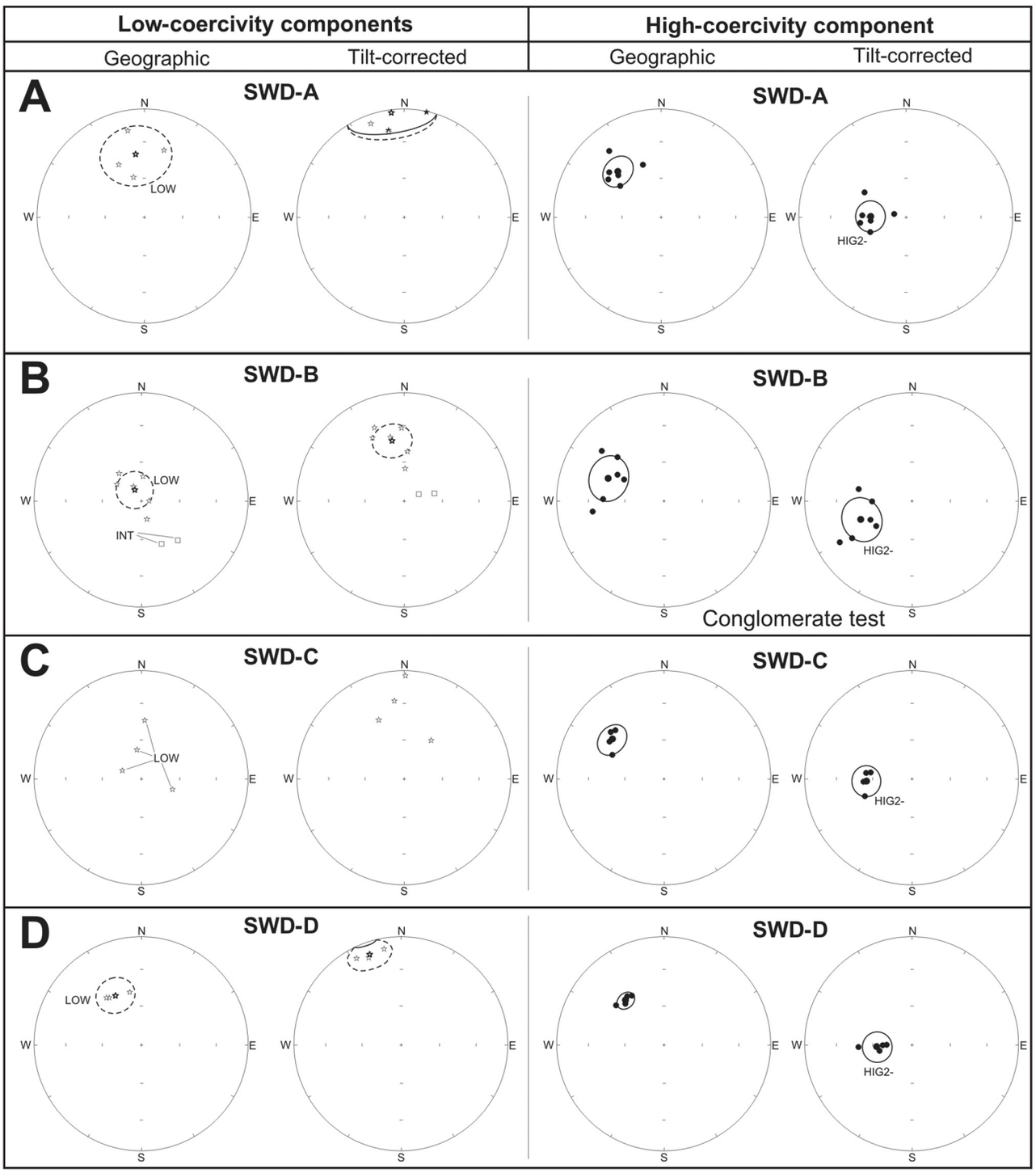

Figure 11. Equal area plots of results from the SWD locality. Symbols are as in Figure 10. (B) depicts the failed conglomerate test from a breccia flow.

to that described for site SWB and antipodal to the high stability component revealed in the trachytic lava). Within twenty-five meters below the dolerite intrusion a fourth magnetic component (in the temperature range 450°C-650°C) appears in the shale and mudstone samples. This direction (labeled "VAR?") is directed northwesterly, at a moderate angle and downwards (Figure 12 and 13a). The dolerite intrusion itself (samples ABP 66-70) is characterized by two magnetic components. A LOW direction is revealed through demagnetization below 450°C, and from that level to 580°C is a steep down north-northwesterly component (abbreviated "DOL"). This DOL direction is similar to the WD direction reported by Hanson *et al.* (2004a) from the same dolerite intrusion at Bakker's Pass and other dolerites with similar ages (~1.87 Ga) intruding the Waterberg Group.

Figure 12 shows examples of demagnetization behavior of three shale samples. Sample ABP 12 comes from ~36 m below the dolerite, while the other two

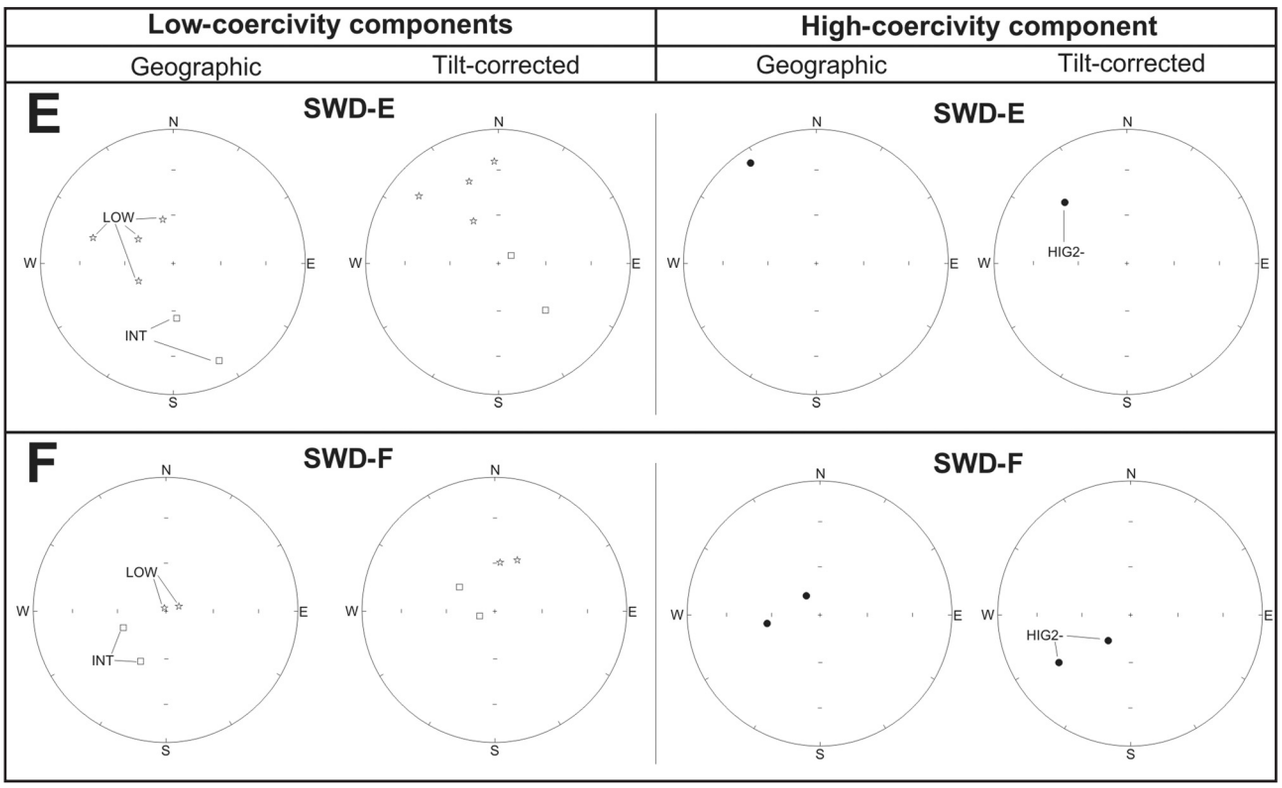

Figure 11. Equal area plots of results from the SWD locality. Symbols are as in Figure 10. (B) depicts the failed conglomerate test from a breccia flow.

(ABP 45 and 60) originate respectively from about 22 m and 5 m below the dolerite. The demagnetization behavior of one dolerite sample (ABP 70) is also shown. The HIG2+ component is partially or completely overprinted by the northwesterly-down (VAR?) direction in samples closer to the dolerite, but shale sampled at greater distance appears unaffected. The scatter of the VAR? directions (approximated by the inverse of the grouping, 1/k = 0.08) is greater than that of the HIG2+ and DOL directions (0.05 and 0.01 respectively). The increased scattering of directions within proximity to the intrusion can be explained by the addition of the differing HIG2+ (high-coercivity remanence in unaffected shale) and DOL (high-coercivity remanence as recorded in the dolerite samples) vectors. This behavior is expected in the warmed zone surrounding an intrusion as described by Irving (1964), an idea that is still regarded as valid today (McElhinny and McFadden, 2000). This constitutes a positive baked-contact test and provides evidence that the HIG2+ shale magnetization has been stable at least since the time of dolerite intrusion at 1872 Ma.

The Nylstroom sill, another post-Waterberg intrusion, was sampled at two sampling sites but yielded no usable results. Anomalously high coercivities revealed during demagnetization and the randomly scattered nature of directions point to lightning strikes as the possible cause of the poor quality of the results. Maré *et al.* (2006) also observed this pervasive lightning signature among their sites within the same intrusion.

SKIL (Shale clasts)

Clasts of shale from the Alma Formation, within a conglomerate in the Skilpadkop Formation along a roadcut in the gorge of Jan Trichardt's Pass, reveal similar magnetic histories to samples of the shale from Bakker's Pass farther west (ABP 1-65). The LOW (low temperature) partial overprint directions and INT (intermediate temperature) directions group well in geographic coordinates (Figure 13b). The high-coercivity components (from only those specimens that displayed consistent behavior at lower demagnetization levels, see Figure 13b) are uniformly ("randomly") oriented (Watson, 1956). This is a positive conglomerate test for the HIG2+ high-temperature component that is recorded in shale and mudstone of the Alma Formation.

Aasvoëlkop Formation

ABP 71-78 (Shale and mudstone)

Red mudstone and shale samples of the Aasvoëlkop Formation were also collected from this western region, directly upsection from site SKIL in the plains north of Jan Trichardt's Pass (Figure 2). These samples yielded results that are similar to the shale and mudstone samples of the Alma Formation, although the Aasvoëlkop is generally less stable (Figure 13c). Three remanence components were revealed by demagnetization. The LOW overprint is not as well developed (only recorded by two samples, in each case below 450°C), but an INT direction and HIG2+ component are better defined (Figure 13c and Table 1).

Table 2. Summary of Field Tests for Stability of High Temperature Components

HIG1		
Fold Test SWF-A (Figure 6a)		
KR fold test (McElhinny, 1964)	= Indeterminate	k_G/k_{TC} = 1.45<[3.44] for 5 linear components. k_G = $k_{TC.}$ Critical values for 95% confidence is given in square brackets.
Fold test (McFadden, 1990)	= Indeterminate	"Xi1"$_{(geographic\ mean)}$ = 2.08<[2.61] for 5 linear components. Geographic mean is not correlated to bedding. "Xi1"$_{(tilt\text{-}corrected\ mean)}$ = 1.48<[2.61] for 5 linear components. Tilt-corrected mean is not correlated to bedding "Xi2"$_{(geographic\ mean)}$ = 3.45>[2.61] for 5 linear components. Geographic mean is correlated to bedding "Xi2"$_{(tilt\text{-}corrected\ mean)}$ = 1.90<[2.61] for 5 linear components. Tilt-corrected mean is not correlated to bedding Optimal clustering at 65% unfolding
DC fold test (Enkin, 2003)	= Indeterminate	|s| = 0.65 < Ds = 0.81, s = 0 cannot be rejected. Where s is the DC slope and Ds is the uncertainty to the slope. |s-1| = 0.35 < Ds = 0.81, s = 1 cannot be rejected. Optimal clustering at 64.8% ± 80.8% unfolding
Fold Test SWF-H (Figure 6b)		
KR fold test (McElhinny, 1964)	= Indeterminate	k_G/k_{TC} = 1.99<[2.97] for 6 linear components. k_G = k_{TC}. Critical values for 95% confidence is given in square brackets.
Fold test (McFadden, 1990)	= Positive	"Xi1"$_{(geographic\ mean)}$ = 2.96>[2.86] for 6 linear components. Geographic mean is correlated to bedding. "Xi1"$_{(tilt\text{-}corrected\ mean)}$ = 0.33<[2.86] for 6 linear components. Tilt-corrected mean is not correlated to bedding "Xi2"$_{(geographic\ mean)}$ = 4.22>[2.86] for 6 linear components. Geographic mean is correlated to bedding. "Xi2"$_{(tilt\text{-}corrected\ mean)}$ = 1.37<[2.86] for 6 linear components. Tilt-corrected mean is not correlated to bedding Optimal clustering at 85% unfolding
DC fold test (Enkin, 2003)	= Positive	|s| = 0.84 > Ds = 0.19, s = 0 can be rejected. Where s is the DC slope and Ds is the uncertainty to the slope. |s-1| = 0.16 < Ds = 0.19, s = 1 cannot be rejected. Optimal clustering at 84.0% ± 18.9% unfolding
Conglomerate Test SWF-D (Figure 5d)		
Randomness (Watson, 1956)	= Positive	R = 1.88<[2.28] for 3 linear components
HIG2+; HIG2-		
Reversals Test SWB (Figure10)		
Reversals test (McFadden and McElhinny, 1990)	= Indeterminate	W-down Direction: Decl.: 241.5, incl.: 56.8, k= 12.59, N= 4 E-up Direction: Decl.: 82.0, incl.: -47.3, k= 16.09, N= 7 Too few directions for common distribution test. Use bootsrap test. l = 15.7°<[24.31]
Conglomerate Test SWD-B (Figure 11b)		
Randomness (Watson, 1956)	= Negative	R = 5.72>[3.95] for 6 linear components
Reversals Test SWB and SWD combined		
Reversals test (McFadden and McElhinny, 1990)	= Positive	"C" quality W-down: Decl.: 262.2, incl.: 55.9, k= 16.0, N= 25 E-up Direction: Decl.: 82.0, incl.: -47.3, k= 16.09, N= 7 PASSES common distribution test. Use analytical test (assume identical k's). l = 8.66°<[11.48]
Baked contact test ABP (Figure 12)		
Baked contact test (Irving, 1964)	= Positive	"A"-type baked contact test
Conglomerate Test SKIL (Figure 13b)		
Randomness (Watson, 1956)	= Positive	R = 3.10<[3.95] for 6 linear components

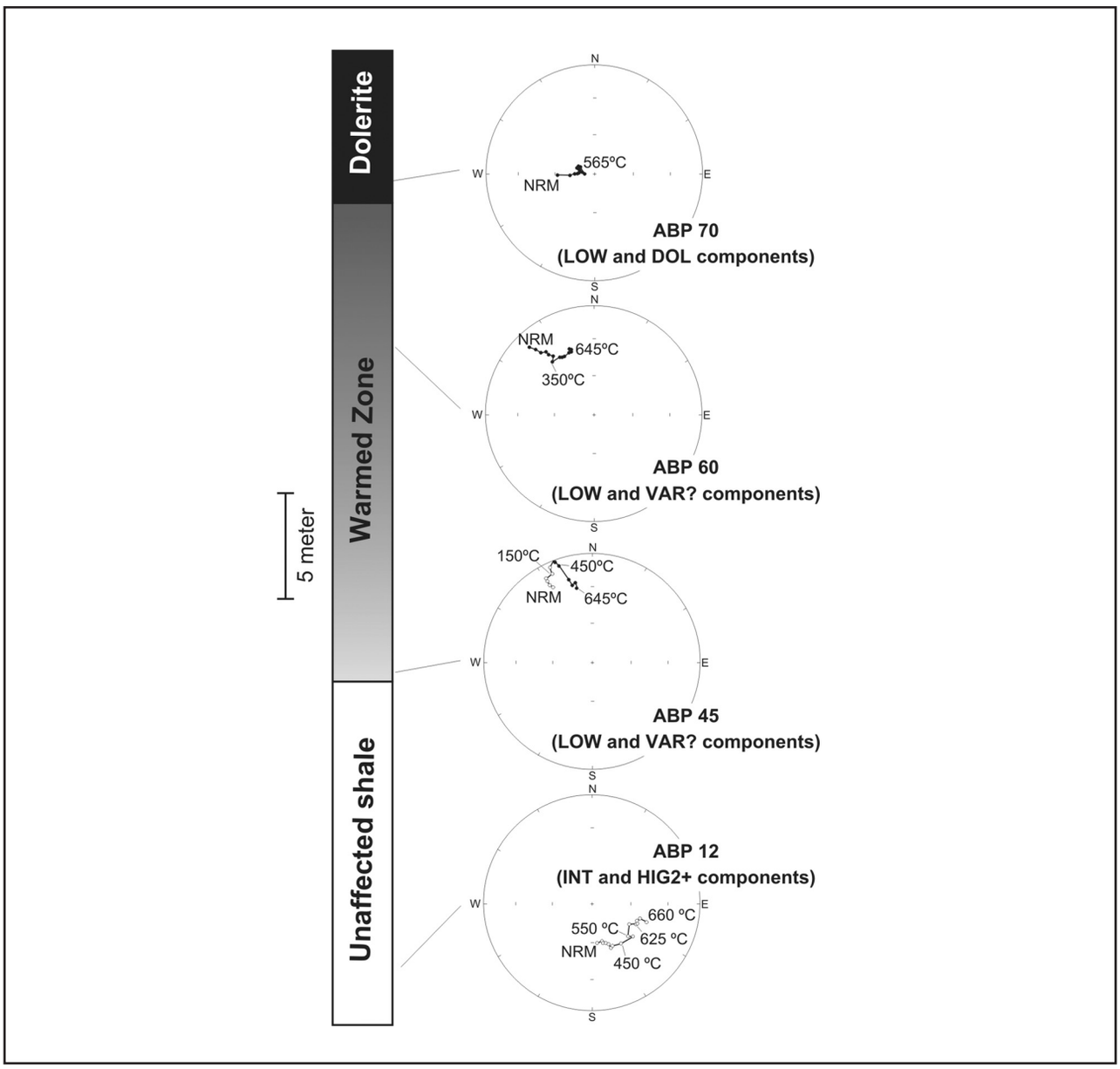

Figure 12. Demagnetization behavior of samples from Bakker's Pass. Equal area projections of demagnetization behavior of shale samples nearing a dolerite intrusion are shown as well as demagnetization of the dolerite itself. Shale from ~23 m below the dolerite intrusion is unaffected, while shale closer to the intrusion displays vector addition between the differing DOL component of the dolerite and HIG2+ primary magnetization of the shale.

In these samples, the HIG2+ direction is slightly more northerly than observed at localities ABP, SWD, and SWB.

Discussion

Mean paleomagnetic directions and interpretation of remanence acquisition

Site means for separate sampling sites were included in the calculation of mean paleomagnetic directions (Figure 14) and poles (Table 3). The following conditions were required for inclusion in pole calculations:

a) the site mean is based on five or more samples,
b) Fisher's (1953) precision parameter (k) for the site mean is above seven, and
c) the α_{95} cone of confidence about the mean is below twenty. The site mean for the VAR? (dolerite overprint) component as recorded in shale samples from Bakker's Pass was excluded because our data essentially duplicate the paleomagnetic results from the same site by Hanson *et al.* (2004a).

At nearly all the sampling sites a north and upward-directed LOW component was revealed usually during low-temperature demagnetization steps. This direction has either a steep, ~60° or higher, inclination (site SWF-A, SWF-E, SWD-B, ABP 1-65 and SKIL), or a moderate (~40°) inclination (site SWC-A, SWC-B, SWD-D and ABP 66-70). When steep, it is parallel to the present geomagnetic field at the sampling localities, but

Table 3. Mean Magnetic Directions and Paleomagnetic Poles

Component	N	Mean Declination (deg)	Mean Inclination (deg)	k	α95	Latitude °N	Longitude °E	K	A95	Time of remanance aquisition
Secondary										
INT	6	172.7	-55.0	71.3	8.0	28.7	21.4	53.9	9.2	post 1.9 Ga
Primary										
HIG2+ and HIG2- HIG2+ and HIG2- combined (this study)	6	263.1	52.5	67.6	8.2	-18.6	327.7	55.0	9.1	
WUBS-II (above + site F, G, I and L*	10	274.2	51.4	33.0	8.5	-10.5	330.4	25.0	9.8	2.05-1.93 Ga
HIG1 (this study)	6	20.1	39.0	19.2	15.7	38.2	53.5	17.0	16.7	
WUBS-I (above + site J, K and M*	9	19.1	41.8	25.1	10.5	36.5	51.3	23.4	10.9	2.05 Ga

* sites F, G, I, J, K, L and M from Jones and McElhinny (1967)

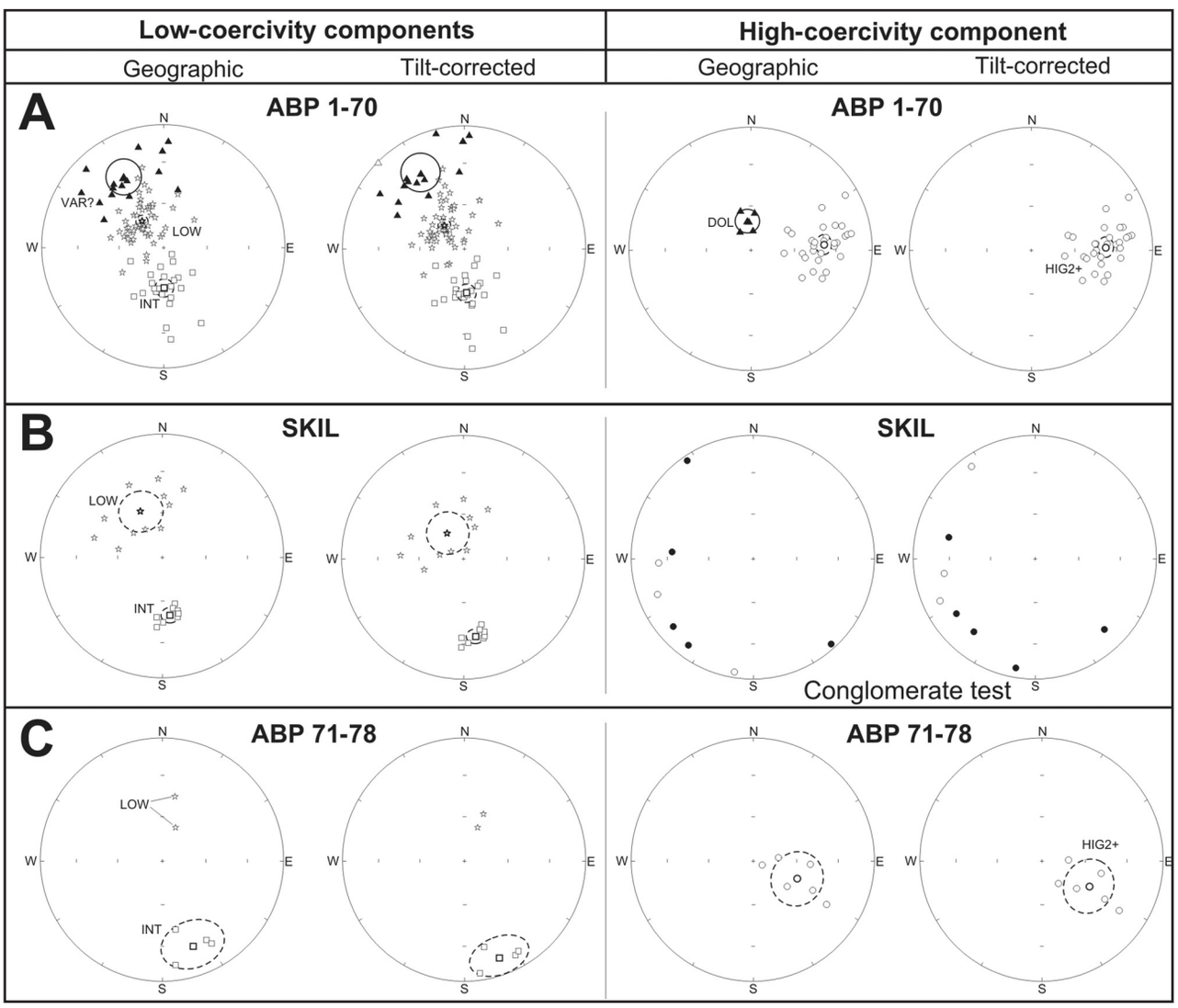

Figure 13. Equal area plots of results from (**A**) the Alma Formation and dolerite intrusion sampled at Bakker's Pass, (**B**) the Skilpadkop Formation (SKIL) conglomerate test and (**C**) the few samples from the Aasvoëlkop Formation. Symbols are all as in Figure 10, but Upward Triagle = VAR? or DOL components.

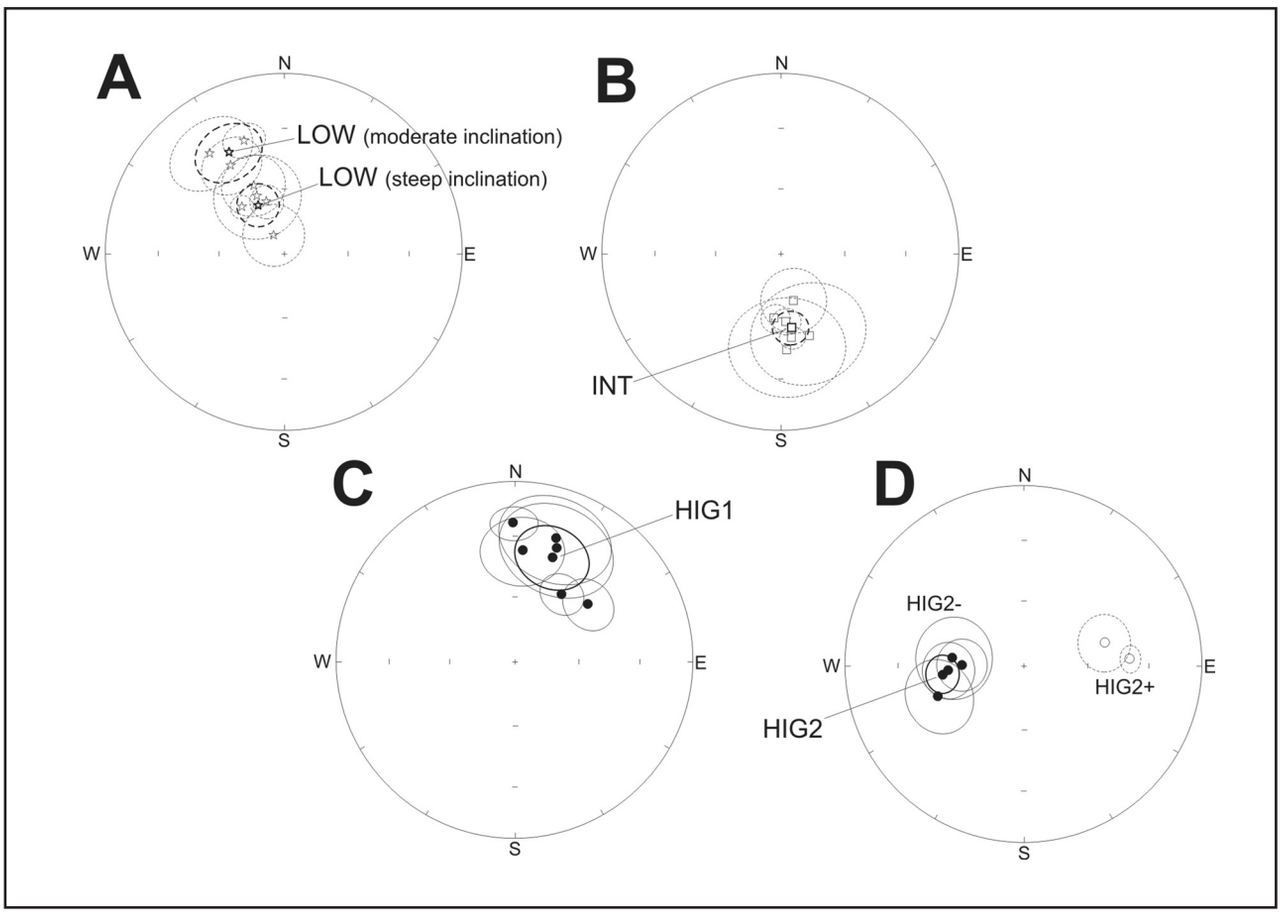

Figure 14. Summary equal area plots of site mean directions of magnetic overprints (**A** and **B**) and primary remanent magnetizations (**C**-**D**). Light ovals = 95 percent confidence for individual sample site, Dark ovals = 95 percent confidence for site mean.

corresponds to the time averaged geomagnetic dipolar field where the inclination is more moderate (Figure 14a).

The intermediate temperature SSW-up (INT, Figure 14b) component was observed at all of the sampling localities, although not in all the samples. It was acquired after folding of the Nylstroom Subgroup and deposition of the Skilpadkop Formation at the base of Waterberg unconformity-bounded sequence III, since it fails both the fold and conglomerate tests. A similar component (D = 179.8°; I = -38.3°) is described by Hanson *et al.* (2004a) as a low-coercivity (overprint) component from dolerite at Bakker's Pass. Hanson *et al.* (2004a) attributed this direction to remagnetization during the Umkondo igneous event at ~1.1 Ga. However, Umkondo directions are typically very shallow (Hargraves *et al.*, 1994) and more like the directions shown by Hanson *et al.* (2004b) for dolerite intrusions from Botswana. The paleomagnetic pole for the INT component is straddled by the poles of the Pilanesberg dykes (Gough, 1956) and that of the Premier kimberlite cluster (Doppelhammer and Hargraves, 1994) and 1244 ± 30 Ma (Onstott *et al.*, 1986) Namaqua Eastern Zone combined pole (Evans *et al.*, 2002). We thus suspect that it is not related to the Umkondo igneous event, but rather to the intrusion of the Pilanesberg dykes, which form a northwest to southeast trending dike swarm that has been observed ~35 km southwest of sampling area. This interpretation suggests an age of ~1.3 Ga to ~1.2 Ga for the INT component. Note that the INT direction cannot be distinguished from the direction obtained by Maré *et al.* (2006) from red beds of the Swaershoek and Wilgeriver Formations, and that those authors rightly interpreted it as being a magnetic overprint.

A positive fold test proves the primary nature of the HIG1 (northwest-down high-temperature, Figure 14c) component as revealed in the lower portion of the Swaershoek Formation, despite the relative high α_{95} value of the calculated mean and corresponding paleomagnetic pole. The calculated paleomagnetic pole (38.2° north, 053.5° east, K = 17.0, A_{95} = 16.7) is statistically indistinguishable from the W1 Waterberg pole (McElhinny, 1968), which is based on site means by Jones and McElhinny (1967) from the Middelburg area (their sites J and K) and flat-lying sedimentary rocks in the vicinity of Bela-Bela (their site M). We have, therefore, combined our six sites with the three sites of Jones and McElhinny (1967) to generate a grand mean pole at (36.5° N, 051.3° E, K = 23.4, A_{95} = 10.9) for the first unconformity-bounded sequence of the Waterberg Group ("WUBS-I"). The 2054 ± 4 Ma age of the quartz porphyry near the base of the Swaershoek Formation (Dorland *et al.*, 2006) is assigned to our WUBS-I pole.

Table 4. Selected Paleoproterozoic Paleomagnetic Poles[a]

Rock Unit	Abbreviation	Age (Ma)	Latitude, °N	Longitude, °E	K	dp in deg.	dm in deg.	Reference[b]
Ongeluk lava	ONG	2222 ± 13	-00.5	100.7	38.3	5.3	5.3	1
Mamatwan-type ore, comp. 1	MAM-1	~2200?	-08.2	111.1	–	5.6	11.1	2
Basal Gamagara/Mapedi	BGM	2060-2200	02.2	081.9	–	7.2	11.5	1
Phalaborwa 1	PB1	2061 ± 0.6	35.9	044.8	–	6.9	10.5	1
Lower Swaershoek Fm.	WUBS-I	2054 ± 4	36.5	051.3	23.4	10.9	10.9	this study
Vredefort VGP	VRED	2023 ± 4	22.3	040.7	–	11.6	15.7	1
Bushveld main + upper	BVMU	–	11.5	027.2	19.0	4.0	4.0	1
Witwatersrand overprint	WITS	1945 ± 40?	19.1	045.6	22.1	7.8	7.8	1
Limpopo metamorphics "A"	LMA	1950-1980?	26.1	022.3	–	7.9	10.3	1
Upper Swaershoek/Alma Formations	WUBS-II	1930-2054	-10.5	330.4	25.0	9.8	9.8	this study
Hartley lava	HAR	1928 ± 4	12.5	332.8	18.6	16.0	16.0	1
Mashonaland sills	MASH	1830 ± 230	07.6	338.2	28.3	5.1	5.1	1
Mamatwan-type ore, comp. 2	MAM-2	–	12.1	321.8	–	3.4	6.0	2
Post-Waterberg intrusions	WSD	1872-1879	28.4	002.6	15.3	11.0	11.0	3
Sand River Dykes	SRD	1876 ± 73?	02.3	009.1	–	10.3	10.3	1
Phalaborwa 2	PB2	1800-1900?	04.2	357.8	31.2	8.8	8.8	1
Post-Bushveld dolerite dykes (eastern Bushveld Complex)	PBD	1649 ± 10 or ~1900?	08.7	022.0	–	18.0	20.6	4

[a]Abbreviations: K, Fisher's (1953) precision parameter in pole space; dp, dm, semiaxes of 95% cone about mean; deg., degrees.
[b]References: (1) Listed by Evans *et al.* (2002); (2) Evans *et al.* (2001); (3) Hanson *et al.* (2004a); (4) Letts *et al.* (2005)
[c]Pole is used in present coordinates

The newly calculated ~2.05 Ga WUBS-I pole rates a five out of a maximum of seven on the "Q" scale of reliability (Van der Voo, 1990). The two criteria that are not met are that our sample set does not show magnetic reversals and the WUBS-I pole shows some similarity to younger paleopoles, *i.e.* the Mesoproterozoic Premier kimberlite pole (Doppelhammer and Hargraves, 1994) and a virtual geographic pole (VGP) for the Ezelfontein Formation of the lower Koras Group (Briden *et al.*, 1979).

In contrast to this pole of the "lower" Swaershoek Formation (WUBS-I), samples from the "upper" Swaershoek Formation and the Alma Formation (WUBS-II) display a dual polarity component (Figure 14d) that unblocks at high temperature demagnetization steps. The HIG2+ (east and up) and HIG2- (west and down) directions pass the reversals test, a conglomerate test and an inverse baked contact test, indicating a remanence acquired before the deposition of the Skilpadkop Formation and before 1.87 Ga, the age of the post-Waterberg intrusion at Bakker's Pass. If the Skilpadkop and the Mannyelanong Hill Formations can both be correlated into Waterberg unconformity-bounded sequence III (Figure 1), then 1.927 Ga sills intruding the latter unit in Botswana (Hanson *et al.*, 2004a) provide a tighter minimum age for the HIG2+/- remanence. We caution, however, that this is a long-distance correlation in stratigraphically complex rocks that may be significantly time-transgressive. The paleomagnetic pole calculated from the HIG2+/- direction (-18.6° N, 327.7° E, K = 55.0, A_{95} = 9.1) is far from the ~2.05 Ga WUBS-I paleomagnetic pole for the "lower" Swaershoek Formation, but it is similar to the W3 pole of McElhinny (1968). Our 6 sites were combined with the four sites from which the W3 pole was calculated (Jones and McElhinny, 1967), to produce a grand mean pole (WUBS-II) at -10.5° N, 330.4° E, K = 25.0, A_{95} = 9.8. On the Q-scale (Van der Voo, 1990) this new pole scores a six out of seven. It fails the numerical age criterion (acquisition of remanence is at best constrained between 2.05 and possibly 1.93 Ga).

Paleoproterozoic Apparent Polar Wander

The apparent polar wander path (APWP) for the Kaapvaal craton during the Paleoproterozoic was reviewed by Evans *et al.* (2002). The only additional poles that have since become available are from Mamatwan-type manganese ores reported by Evans *et al.* (2001) (the 2002 article had an extensively delayed publication), from 1.87 Ga post-Waterberg dolerite intrusions and lavas (Sibasa and Nzhelele Formations) and dolerite sills in the Soutpansberg Group reported by Hanson *et al.* (2004a), and from mafic dykes that intrude the eastern Bushveld Complex (Letts *et al.*, 2005). These results are briefly reviewed here and, together with the poles from this study, are used to reevaluate the Paleoproterozoic APWP of the Kaapvaal craton.

Evans *et al.* (2001) sampled progressively enriched manganese ores at three working mines in the Kalahari manganese field. Their study identified three distinct remanent directions and confirmed multistage development of manganese ores. Two of these remanent directions were identified in the older Mamatwan-type ores. An early diagenetic remanence (named MAM-1) is similar to a previous result from the immediately underlying Ongeluk lavas (Evans *et al.*, 1997) and was identified together with a late diagenetic or weak metamorphic overprint (named MAM-2) that

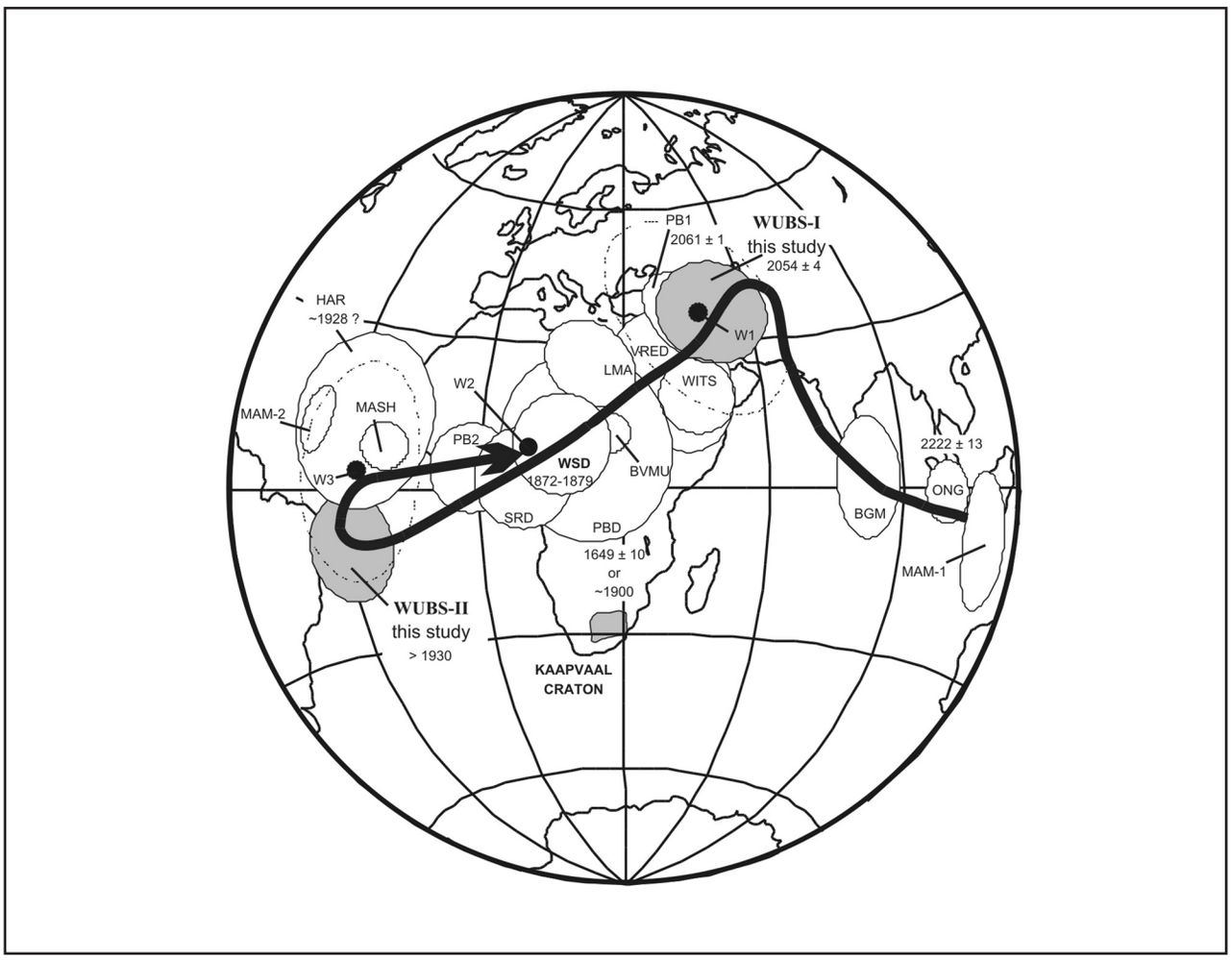

Figure 15. Paleoproterozoic APWP for the Kaapvaal craton, with new poles WUBS-I (high-temperature component for the lower part of Swaershoek Formation) and WUBS-II (dual polarity high-temperature component from the upper part of the Swaershoek Formation and the Alma Formation) shaded. Outline of the continents and the Kaapvaal craton are shown for reference. Solid swath shows APWP for the time interval 2.2 Ga to 1.9 Ga. ONG = Ongeluk lavas, MAM-1 = Mamatwan type manganese ores component 1, BGM = Basal Gamagara/Mapedi, PB1 = Phalaborwa Group 1, W1 = Lower Waterberg (Morgan and Briden, 1981), WITS = Witwatersrand overprint, VRED = Vredefort VGP, BVMU, Bushveld Main and Upper Zones combined, LMA, Limpopo metamorphics A component, W3 = Upper Waterberg (Morgan and Briden, 1981), SRD = Sand River dikes, WSD = Post-Waterberg dolerites and Soutpansberg mafic rocks, W2 = Nzelele Formation *see text* (Morgan and Briden, 1981), PB2 = Phalaborwa Group 2, MASH = Mashonaland sills, HAR = Hartley lavas, MAM-2 = Mamatwan type manganese ores component 2 and PBD = dolerites intruding the Eastern Bushveld Complex. For details of the poles see the discussion and Table 4. Note that poles W1 and W3 are depicted as points with dashed ovals. VGP W2 is depicted just as a point.

resembles poles from the ~1.9 Ga Hartley lavas and Mashonaland sills (see references cited in Table 4) and could possibly be related to ~1.8 to ~1.7 Ga deformation in the Kheis terrane (Evans *et al.*, 2001).

Hanson *et al.* (2004a) sampled lavas of the Sibasa (LB1) and Nzelele Formations (NB1) together with dolerite sills (denoted SD) in the Soutpansberg area. This was done to test if the Soutpansberg mafic rocks were emplaced in the same mafic event as the ~1.88 Ga post-Waterberg dolerite sills. The directions obtained by Hanson *et al.* (2004a) from two lava flows (Sibasa and Nzhelele Formation) and five dolerite sills are antipodal to the 1.87 Ga WD directions. The site directions (both polarities) were combined by Hanson *et al.* (2004a) and used to calculate a grand mean pole (WSD). The assumption by Hanson *et al.* (2004a) that the WD group and SD-LB1-NB1 group of remanence directions are representative of the same ~1.88 Ga old mafic event is based solely on the antipodality of the directions. This assumption may be reasonable given the antipodality and geographic proximity of the rocks, but without any other age constraints it is questionable. The Kaapvaal craton might have been relatively immobile at this stage translating into a constant pole position (but allowing for one or several reversals of the Earth's magnetic field and a considerable amount of time). Another possibility might be that of an APWP loop, but this speculation would require further testing.

Mafic dykes that intrude the eastern Bushveld Complex were sampled recently by Letts *et al.* (2005) for both paleomagnetic and $^{40}Ar/^{39}Ar$ analyses. Both

techniques suggest these dykes, which were previously thought to be Jurassic, are in fact Precambrian in age. A positive reversals test and a semi-conclusive baked contact test were used to demonstrate the primary nature of the remanence (Letts *et al.*, 2005). When compared to other poles from the Kaapvaal craton (Table 4 and Figure 15), an age of ~1.9 Ga is suggested for the pole of Letts *et al.* (2005) (coded here as PBD), but this is in contrast to the $^{40}Ar/^{39}Ar$ age of 1649 ± 10 Ma that Letts *et al.* (2005) report. These authors concluded that either the 1.65 Ga $^{40}Ar/^{39}Ar$ age is a primary cooling age, and that there is an apparent polar wander loop with the 1.9 Ga and 1.65 Ga poles of the Kaapvaal craton being virtually identical, or that the $^{40}Ar/^{39}Ar$ age represents a thermal disturbance, which did not erase the 1.9 Ga primary magnetic signature. Unfortunately there are no well-established poles for the Kaapvaal craton in the interval ~1.9 Ga to ~1.3 Ga and the possibility of an APWP loop at 1.65 Ga can only be confirmed or refuted pending more isotopic and paleomagnetic studies.

The poles from this study are listed (Table 4) and plotted (Figure 15) together with the previously published paleomagnetic poles for the Kaapvaal craton during the Paleoproterozoic (as listed by Evans *et al.*, 2002) and the two poles reviewed above to reveal a APWP that is for the most part consistent with the generally accepted swath from a low latitude position west of Africa (Ongeluk and MAM-1 poles), across the Arabian Peninsula and north-east Africa (Phalaborwa Group 1 pole) and generally towards the west coast of Africa in the later part of the Paleoproterozoic. However, there are some previously unrecognized complexities.

The ~2.05 Ga WUBS-I pole of this study overlaps very well with the ~2.06 Ga (Reischmann, 1995) Phalaborwa Group 1 (PB1) pole of Morgan and Briden (1981), but does not compare well with the combined Bushveld Main and Upper zone poles of Evans *et al.* (2002), despite coeval U-Pb zircon ages of Bushveld magmatism (see Walraven, 1997). Following the suggestion in Evans *et al.* (2002), we suggest that the Bushveld Complex had a long cooling and/or hydrothermal history and substantially delayed magnetic remanence acquisition following its crystallization. Long-lived fluid flow events (continuing up to ~100 Myr after intrusion) have in fact been suggested, as indicated by $^{40}Ar/^{39}Ar$ geochronology for some Bushveld granites (Robb *et al.*, 2000). Some rocks adjacent to the Bushveld Complex also bear witness to these late thermal events (Kruger *et al.*, 1998). The exact time of magnetic remanence acquisition is unknown, and particularly difficult to constrain given the likelihood that this process did not occur simultaneously in different parts of the intrusion. The age of the WUBS-I pole is thus much better constrained than those of the Bushveld Igneous Complex, and in our opinion the WUBS-I pole is a better representation of the position of the Kaapvaal craton during the final stages of Bushveld intrusion.

After ~2.05 Ga the Kaapvaal APWP shifts steadily southwest, embracing the ~2.02 Ga combined Vredefort virtual geographic pole of Hargraves (1970) and Hart *et al.* (1995), as reported by Evans *et al.* (2002), as well as the poorly dated ~2.02 to ~1.97 Ga Limpopo metamorphics "A" pole of Morgan (1985). Moving from the WUBS-I pole to the WUBS-II pole from the "upper" Swaershoek and overlying Alma Formation, a large shift occurs in the APWP from northeast Africa to a position on the east coast of Brazil. This southwesterly drift took place before ~1.88 Ga (the age recorded by some post-Waterberg dolerite sills (Hanson *et al.*, 2004a)), as illustrated by the positive inverse baked contact test at Bakker's Pass. The positions of the ~1.93 Ga Hartley lava pole, poorly dated Mashonaland sills pole and MAM2 pole, are slightly to the north of WUBS-II. Recall that our preliminary data from the Aasvoëlkop Formation—too few for robust calculation—hint at a WUBS-III pole position in that more northerly location.

A previously unrecognized loop in the APWP is revealed by the WUBS-I pole, through the WUBS-II pole and back to the ~1.88Ga WSD pole, which may or may not be corroborated by the pole of Letts *et al.* (2005) from mafic dykes intruding the eastern Bushveld Complex (PBD).

Implications for red bed stratigraphy and correlation in southern Africa

The considerable amount of continental motion recorded by paleomagnetic directional discrepancies between the Lower Swaershoek Formation and the overlying Upper Swaershoek and Alma Formations casts doubt on the conformable nature of the Lower and Upper Swaershoek as inferred by Jansen (1982) and other workers. Our paleomagnetic results thus generally support the suggestion by Cheney and Twist (1986) that a major unconformity is present within the Swaershoek Formation. Precise placement of that lacuna, however, remains uncertain. Dorland *et al.* (2006) preferred a lower sequence boundary for WUBS-II at the prominent conglomerate which we have sampled as site SWF-E. However, we observe a paleomagnetic remanence similar to WUBS-I as a local overprint at that site, and also as a component of unknown age in the overlying section SWE. If these sites are within WUBS-II as postulated by Dorland et al. (2006), then their north-down direction must be a substantially later overprint, perhaps acquired after the APWP return loop to poles WSD and PBD. Alternatively, the local SWF-E overprint might manifest earliest diagenetic or low-grade hydrothermal fluids accompanying the waning stages of Bushveld magmatism, and WUBS-I approximate the time of deposition for these and overlying SWE strata. In this case, the base of WUBS-II should be found higher in the section. We encourage more thorough paleomagnetic studies of the Nylstroom basin in order to trace the APWP shift across the outcropping strata, as a potential proxy for this cryptic sequence boundary within the lower Waterberg Group. Such a study would help characterize base-level changes, and hence

landscape evolution, during post-Bushveld crustal stabilization.

Conclusions

Our results from redbeds and volcanics of the Nylstroom Subgroup and post-Waterberg intrusions confirm the established form of the Paleoproterozoic APWP of the Kaapvaal craton, but also highlight some important previously unrecognized complexities. The Lower Swaershoek Formation, which can be correlated to the Rust de Winter Formation (Dorland *et al*., 2006), the Glentig Formation and the Loskop Formation (Cheney and Twist, 1986), records a primary remanence established by a positive fold test. The resulting paleomagnetic pole WUBS-I (36.5° N, 051.3° E, K = 23.4, A_{95} = 10.9) is a better representation of the Kaapvaal craton's position during the closing stages of the intrusion of the Bushveld Igneous Complex than that provided by the existing paleomagnetic poles from the Bushveld Complex itself. The large shift in pole positions observed between the WUBS-I pole of the Lower Swaershoek Formation and Upper Swaershoek Formation WUBS-II pole (located at -10.5° N, 330.4° E, K = 25.0, A_{95} = 9.8) shows that these two rock packages are separated by an unconformity, as first suggested by Cheney and Twist (1986). The primary nature of the remanence in the Upper Swaershoek and Alma Formations is established by a positive reversals test, conglomerate test and an inverse baked contact test. The ~1.88 Ga WSD remanence direction of Hanson *et al*. (2004a) is confirmed by our study and its primary nature is demonstrated by a positive baked contact test. Our results document a previously unrecognized loop in the Kaapvaal APWP between the WUBS-I pole, WUBS-II pole, and post-Waterberg (WSD) pole.

Acknowledgments

The principal author acknowledges support from the South African National Research Foundation (NRF), the Australian Research Council, Agouron Institute of Geobiology, and the David and Lucile Packard Foundation. We thank journal reviewers R.E. Hanson, W.A. Gose and J.L. Kirschvink for their helpful criticisms.

References

Briden, J. C., Duff, B. A. and Kröner, A. (1979). Paleomagnetism of the Koras Group, northern Cape Province, South Africa. *Precambrian Research*, **10**, 43-57.

Callaghan, C. C., Eriksson, P. G. and Snyman, C. P. (1991). The sedimentology of the Waterberg Group in Transvaal, South Africa: an overview. *Journal of African Earth Sciences*, **13**, 107-119.

Cheney, E. S. and Twist, D. (1986). The Waterberg "Basin" - a reappraisal. *Transactions of the Geological Society of South Africa*, **89**, 353-360.

Cogné, J. P. (2003). PaleoMac: a Macintosh™ application for reconstructions. *Geochemistry, Geophysics and Geosystems*, **4**, pp. 1007.

Council for Geoscience (1997). Geological Map of the Republic of South Africa and the Kingdoms of Leshoto and Swaziland. Council for Geoscience, Pretoria.

Doppelhammer, S. K. and Hargraves, R. B. (1994). Paleomagnetism of the Schuller and Franspoort kimberlite pipes in South Africa and an improved Premier pole. *Precambrian Research*, **69**, 193-197.

Dorland, H., Beukes, N. J., Gutzmer, J., Armstrong, R. A. and Evans, D. A. D. (2006). Precise SHRIMP U-Pb zircon age constraints on the lower Waterberg and Soutpansberg Groups, South Africa. *South African Journal of Geology*, **This volume**.

Du Plessis, C. P. (1987). New perspectives on early Waterberg Group sedimentation from the Gatkop area, northwestern Transvaal. *South African Journal of Geology*, **90**, 395-408.

Enkin, R. J. (2003). The direction-correction tilt test: and all-purpose tilt/fold test for paleomagnetic studies. *Earth and Planetary Science Letters*, **212**, 151-166.

Evans, D. A. D., Beukes, N. J. and Kirschvink, J. L. (1997). Low-latitude glaciation in the Palaeoproterozoic era. *Nature*, **386**, 262-266.

Evans, D. A. D., Beukes, N. J. and Kirschvink, J. L. (2002). Paleomagnetism of a lateritic paleoweathering horizon and overlying Paleoproterozoic red beds from South Africa: Implications for the Kaapvaal apparent polar wander path and a confirmation of atmospheric oxygen enrichment. *Journal of Geophysical Research*, **107** (B12), 2326-2333.

Evans, D. A. D., Gutzmer, J., Beukes, N. J. and Kirschvink, J. L. (2001). Paleomagnetic constraints on ages of mineralization in the Kalahari Manganese Field, South Africa. *Economic Geology*, **96**, 621-631.

Fisher, R. A. (1953). Dispersion on a sphere. *Proceedings of the Royal Society of London*, **Ser. A, 217**, 295-305.

Gough, D. I. (1956). A study of the paleomagnetism of the Pilanesberg dykes. *Monthly Notices of the Royal Atronomycal Society, Geophysical Supplement*, **7**, 196-213.

Hanson, R. E., Gose, W. A., Crowley, J. L., Ramezani, J., Bowring, S. A., Bullen, D. S., Hall, R. P., Pancake, J. A. and Mukwakwami, J. (2004a). Paleoproterozoic intraplate magmatism and basin development on the Kaapvaal Craton: Age, paleomagnetism and geochemistry of ~1.93 to ~1.87 Ga post-Waterberg dolerites. *South African Journal of Geology*, **107**, 233-254.

Hanson, R.E., Crowley, J.L., Bowring, S.A., Ramezani, J., Gose, W.A., Dalziel, I.W.D., Pancake, J.A., Seidel, E.K., Blenkinsop, T.G. and Mukwakwami, J. (2004b). Coeval large-scale magmatism in the Kalahari and Laurentian Cratons during Rodinia assembly. *Science*, **304**, 1126-1129.

Hargraves, R. B. (1970). Paleomagnetic evidence relevant to the origin of the Vredefort Ring. *Journal of Geology*, **78**, 253-263.

Hargraves, R. B., Hattingh, P. J. and Onstott, T. C. (1994). Paleomagnetic results from the Timbavati Gabbros in the Kruger National Park, South Africa. *South African Journal of Geology*, **97**, 114-118.

Hart, R. J., Hargraves, R. B., Andreoli, M. A. G., Tredoux, M. and Doucouré, C. M. (1995). Magnetic anomaly near the center of the Vredefort structure: Implications for imact-related magnetic signatures. *Geology*, **23**, 277-280.

Irving, E. (1964). Paleomagnetism and its Implication to Geological and Geophysical Problems. Wiley, New York, 399 pp.

Jansen, H. (1982). The Geology of the Waterberg Basins in the Transvaal, Republic of South Africa, Memoir of the Geological Survey of South Africa, **71**, 98pp.

Jones, C. H. (2002). User-driven integrated software lives: "Paleomag" Paleomagnetic analysis on the Macintosh™. *Computers and Geosciences*, **28**, 1145-1151.

Jones, D. L. and McElhinny, M. W. (1967). Stratigraphic interpretation of paleomagnetic measurements on the Waterberg Red Beds of South Africa. *Journal of Geophysical Research*, **72**, 4171-4179.

Kirschvink, J. L. (1980). The least squares line and plane and the analysis of palaeomagnetic data. *Geophysics Journal of the Royal Astronomical Society*, **62**, 699-718.

Kruger, F. J., Kamber, B. S. and Harris, P. D. (1998). Isotopic peculiarities of an Archaean pegmatite (Union Mine, Mica, South Africa), geochemical and geochronological implications. *Precambrian Research*, **91**, 253-267.

Letts, S., Torsvik, T. H., Webb, S. J., Ashwal, L. D., Eide, E. A. and Chunnett, G. (2005). Paleomagnetism and $^{40}Ar/^{39}Ar$ geochronology of mafic dykes from the eastern Bushveld Complex (South Africa). *Geophysical Journal International*, **162**, 36-48.

Maré, L. P., Eriksson, P. G. and Améglio, L. (2006). A paleomagnetic study of the lower part of the Paleoproterozoic Waterberg Group, South Africa. *Journal of African Earth Sciences*, **44**, 21-36.

McElhinny, M. W. (1964). Statistical significance of the fold test in palaeomagnetism. *Geophysics Journal of the Royal Astronomical Society*, **10**, 375-381.

McElhinny, M. W. (1968). Notes on progress in geophysics: Paleomagnetic directions and pole positions-IX. *Geophysical Journal of the Royal*

Astronomical Society, **16**, 207-224.

McElhinny, M. W. and McFadden, P. L. (2000). Paleomagnetism: Continents and oceans. Academic Press, London, 386 pp.

McFadden, P. L. (1990). A new fold test for palaeomagnetic studies. *Geophysics Journal International*, **103**, 163-169.

McFadden, P. L. and Jones, D. L. (1981). The fold test in paleomagnetism. *Geophysical Journal of the Royal Astronomical Society*, **67**, 53-58.

McFadden, P. L. and McElhinny, M. W. (1988). The combined analysis of remagnetization circles and direct observations in paleomagnetism. *Earth and Planetary Science Letters*, **87**, 161-172.

McFadden, P. L. and McElhinny, M. W. (1990). Classification of the reversals test in palaeomagnetism. *Geophysics Journal International*, **103**, 725-729.

Morgan, G. E. (1985). The paleomagnetism and cooling history of metamorphic and igneous rocks from the Limpopo Mobile Belt, southern Africa. *Geological Society of America Bulletin*, **96**, 663-675.

Morgan, G. E. and Briden, J. C. (1981). Aspects of Precambrian paleomagnetism, with new data from the Limpopo Mobile Belt and Kaapvaal Craton in Southern Africa. *Physics of the Earth and Planetary Interiors*, **24**, 142-168.

Onstott, T. C., Hargraves, R. B., Joubert, P. and Reid, D. L. (1986). Constraints on the tectonic evolution of the Namaqua Province, II, Reconnaissance paleomagnetic and $^{40}Ar/^{39}Ar$ results from the Namaqua Province and Kheis Belt. *Transactions of the Geological Society of South Africa*, **89**, 143-170.

Reischmann, T. (1995). Precise U/Pb age determination with baddeleyite (ZrO_2), a case study from the Palaborwa Igneous Complex, South Africa. *South African Journal of Geology*, **98**, 1-4.

Robb, L. J., Freeman, L. A. and Armstrong, R. A. (2000). Nature and longevity of hydrothermal fluid flow and mineralization in granites of the Bushveld Complex, South Africa. *Transactions of the Royal Society of Edinburgh Earth Sciences*, **33**, 259-282.

SACS, South African Committee for Stratigraphy (1980). Stratigraphy of South Africa. Part 1: Lithostratigraphy of the Republic of South Africa, South West Africa/Namibia and the Republics of Bophuthatswana, Transkei and Venda (Compiled by Kent, L.E.). *Handbook of the Geological Survey of South Africa*, **8**, 690pp.

Van der Voo, R. (1990). The reliability of paleomagnetic data. *Tectonophysics*, **184**, 1-9.

Walraven, F. (1997). Geochronology of the Rooiberg Group, Transvaal Supergroup, South Africa. *Information Circular of the Economic Geology Research Unit, University of the Witwatersrand, Johannesburg, South Africa*, **316**, 21pp.

Watson, G. S. (1956). A test for randomness of directions. *Monthly Notices of the Royal Atronomycal Society, Geophysical Supplement*, **7**, 160-161.

Editorial handling: J. Gutzmer